Integration of Wnt-inhibitory Activity and Structural Novelty Scoring Results to Uncover Novel Bioactive Natural Products: New Bicyclo[3.3.1]non-3-ene-2,9-diones from the Leaves of *Hymenocardia punctata*.

Luis-Manuel Quiros-Guerrero[1,2], Laurence Marcourt[1,2], Nathareen Chaiwangrach[3], Alexey Koval[4], Emerson Ferreira Queiroz[1,2], Bruno David[6], Antonio Grondin[6], Vladimir L. Katanaev[4,5], Jean-Luc Wolfender[1,2*]

[1]Institute of Pharmaceutical Sciences of Western Switzerland, University of Geneva, CMU, 1211 Geneva, Switzerland.
[2]School of Pharmaceutical Sciences, University of Geneva, CMU, 1211 Geneva, Switzerland.
[3]Centre of Excellence in Cannabis Research, Department of Pharmaceutical Chemistry and Pharmacognosy, Faculty of Pharmaceutical Sciences, Naresuan University, Phitsanulok 65000, Thailand.
[4]Department of Cell Physiology and Metabolism, Translational Research Centre in Oncohaematology, Faculty of Medicine, 1211 Geneva, Switzerland.
[5]School of Medicine and Life Sciences, Far Eastern Federal University, 690091 Vladivostok, Russia.
[6]Green Mission Department, Herbal Products Laboratory, Pierre Fabre Research Institute, Toulouse, France.

* Correspondence:
Jean-Luc Wolfender
jean-luc.wolfender@unige.ch

Keywords: Natural products, Wnt-pathway, Wnt-pathway modulators, structural novelty discovery, '*Inventa*' scoring, *Hymenocardia punctata*, Metabolomics (LC-MS), structural elucidation.

Abstract

In natural products (NP) research, methods for the efficient prioritization of natural extracts (NEs) are key for discovering novel bioactive NPs. In this study a biodiverse collection of 1600 NEs, previously analyzed by UHPLC-HRMS^2 metabolite profiling was screened for Wnt pathway regulation. The results of the biological screening drove the selection of a subset of 30 non-toxic NEs with an inhibitory IC$_{50}$ ≤ 5 μg/mL. To increase the chance of finding structurally novel bioactive NPs, *Inventa*, a computational tool for automated scoring of NEs based on structural novelty was used to mine the HRMS^2 analysis and dereplication results. After this, 4 out of the 30 bioactive NEs were shortlisted by this approach. The most promising sample was the ethyl acetate extract of the leaves of *Hymenocardia punctata* (Phyllanthaceae). Further phytochemical investigations of this species resulted in the isolation of three known prenylated flavones (**3**, **5**, **7**) and ten novel bicyclo[3.3.1]non-3-ene-2,9-diones (**1**, **2**, **4**, **6**, **8**-**13**), named *Hymenotamayonins*. Assessment of the Wnt inhibitory activity of these compounds revealed that two prenylated flavones and three novel bicyclic compounds showed interesting activity without apparent cytotoxicity. This study highlights the potential of combining *Inventa*'s structural novelty scores with biological screening results to effectively discover novel bioactive NPs in large NE collections.

Introduction

Nature is a valuable source of chemical diversity, offering a wide range of molecules with therapeutic properties (Newman and Cragg, 2020). Plants serve as important reservoirs of bioactive natural products (NPs) that have been utilized for medicinal purposes for centuries. NPs often exhibit complex chemical structures due to evolutionary processes that enable them to interact with biological targets in precise ways (Feher and Schmidt, 2003; Atanasov et al., 2021). These characteristics are challenging to replicate synthetically, making NPs exceptionally suitable as starting points for drug development (Clark, 1996; Dias et al., 2012; Allard et al., 2023). Natural extracts (NEs) from plant origin possess a vast chemical diversity of NPs, positioning them as highly promising assets for the exploration and advancement of novel therapeutic agents. Although to date, only about *c.a.* 20% of plant species have been investigated, finding novel or rare structural scaffolds is becoming increasingly difficult. This challenge arises because most botanical genera and families have already been studied, and species that are taxonomically related tend to biosynthesize similar constituents (David et al., 2015).

The most common approaches used for the selection of NEs prior to *in-depth* phytochemical studies include high-throughput bioactivity screening, traditional use of given medicinal plants, and literature reports (Hostettmann and Terreaux, 2000; Sarker et al., 2005; Sarker and Nahar, 2012). The identification of the active principles is classically performed by bio guided isolation. This strategy is resource-intensive and time-consuming due to the need for multiple rounds of fractionation and bioassays. There is also a risk of bioactivity lost during the isolation process while other concerns include false positives, selectivity issues in bioassays, and missing synergistic effects (Pieters and Vlietinck, 2005; Hamburger, 2019; Najmi et al., 2022). To overcome certain limitations and anticipate the chances to find bioactive NPs of interest, strategies like structural dereplication and extensive metabolites annotations through metabolomics are increasingly being integrated early in research workflows (Olivon et al., 2017; Caesar et al., 2021).

Early structural identifications of NPs in NEs can assist researchers in avoiding reported active NPs or efficiently searching for analogs of previously reported bioactive NPs (Hubert et al., 2017; Selegato et al., 2023). With the advancement of computational annotations methods throughput in metabolomics, it is now possible to evaluate the chemical space of large NEs collections (Gaudry et al., 2023). This information can be used to prioritize samples in the search for structurally novel NPs (Quiros-Guerrero et al., 2022).

To automatedly mine the large amount of metabolite profiling data and make use of prior pharmacognosy knowledge we recently introduced *Inventa* (Quiros-Guerrero et al., 2022), a metabolomics bioinformatic workflow designed to streamline the NEs selection process. Its primary objective is to pinpoint NEs with a heightened probability of containing structurally novel NPs within NEs collections, that have undergone untargeted UHPLC-HRMS^2 metabolite profiling. *Inventa* follows a structured process and takes as input the results from the MZmine data processing (Schmid et al., 2023), the subsequent MS^2 spectral data organization using Featured-Based Molecular Networking (FBMN) (Nothias et al., 2020), and the MS^2 spectra annotation from advanced computational methods like ISDB (Allard et al., 2016; Rutz et al., 2019), and SIRUS (Dührkop et al., 2019). The annotation results of the features [a peak with an *m/z* value at a given retention time] detected in the samples include molecular formulas, chemical classes based on NPClassifier (Dührkop et al., 2021; Kim et al., 2021), and structural candidates (Dührkop et al., 2015; Cabral et al., 2016). It integrates previous literature reports for the considered taxon by conducting automated searches in the [LOTUS](#) initiative (Rutz et al., 2022), where NP structure occurrences are catalogued in their respective source organisms. Additionally, it exploits the MEMO (Gaudry et al., 2022) spectral fingerprints to evaluate the spectral diversity exhibited by a particular sample within a set of NEs. Based on all these data, *Inventa* calculates four individual component scores: the proportion of annotated features in each NE, the specificity of these features within a NEs data set, the number of reported structures in the NE taxon and the spectral divergence of the individual NE within the data set. It provides a combined score (*Priority Score*, PS) that enables the prioritization of NEs based on their potential for containing structurally novel NPs. In this study we intend to evaluate how *Inventa* can be combined with bioactivity screening results to highlight structurally novel bioactive NPs capable of regulating the Wnt signaling pathway.

The Wnt signaling pathway ([Q155769](#)) is critical in several biological processes like embryonic development, tissue homeostasis, and cellular proliferation (Blagodatski et al., 2020; Boudou et al., 2022; Liu et al., 2022). However, when dysregulated, it has been associated with several disorders, including cancer (Shaw et al., 2019b; Lim et al., 2021; Jiang et al., 2022), Alzheimer's (Inestrosa et al., 2012), and osteoporosis (Houschyar et al., 2018; Lojk and Marc, 2021). Many of the current cancer treatments affect rapidly dividing cells resulting in notable side effects since these cells are essential for tissue maintenance in adults. A more targeted and specific approach, with fewer side effects, may be possible by focusing on targeting the Wnt signaling pathway exclusively in the cancer cells (Shaw et al., 2019b). Several NPs from diverse plant species have been reported to have some activity over the Wnt-signaling pathway through disruption of the Wnt/β-catenin cascade (Pooja and Karunagaran,

2014; Gu et al., 2019). Thus, the discovery of NPs capable of inhibiting or regulating the Wnt-signaling pathway has become a topic of significant interest in drug discovery programs (Fuentes et al., 2015; Nusse and Clevers, 2017).

The collection of NEs used for the screening consists in a subset of 1,600 NEs from the Pierre Fabre Laboratories (PFL) Library that were previously analyzed by massive UHPLC-HRMS^2 metabolite profiling (Allard et al., 2023). The PFL library englobes over 17,000 unique samples and it was registered in April 2020 at the European Commission under the accession number 03-FR-2020, confirming its compliance with the criteria established by the EU ABS Regulation and the Nagoya Protocol (Nagoya Protocol on access to genetic resources and the fair and equitable sharing of benefits arising from their utilization to the convention of biological diversity, 2011).

In the search for structurally novel bioactive NPs from plants, we sought to investigate the UHPLC-HRMS^2 metabolite profiling and Wnt-pathway regulation screening results for this set of 1,600 NEs. Then, to increase the chances of selecting active NEs containing novel NPs, *Inventa* was used to calculate priority scores for structural novelty. The combination of both information, the screening results, and *Inventa*'s scores highlighted several bioactive NEs with a high potential of containing structurally novel NPs.

Results and Discussion

Overview of the Wnt-regulation bioactivity assay results for the 1,600 NEs collection

The same samples used for the UHPLC-HRMS^2 metabolite profiling previously described by Allard et al. (2023) were screened for the presence of compounds with a potential Wnt-regulatory activity. The screening experimental design used the BT-20 triple-negative breast cancer cell line (TNBC), stably transfected with the TopFlash reporter construct, and sensitive to purified Wnt3a stimulation (Koval et al., 2014; Shaw et al., 2019a). The NEs were screened in single repeats at five different concentrations (50, 25, 12.5, 6, and 3 μg/mL) and cytotoxicity was monitored at the same time.

The results of the Wnt-regulatory bioactivity testing showed that out of the 1,600 NEs, 497 exhibited either Wnt-regulatory or cytotoxic activity. Among these active samples, 389 active NEs were classified into 148 NEs Wnt potentiators (79 NEs were non-toxic and 69 NEs had a toxicity IC$_{50}$ > 50 μg/mL), and 241 NEs Wnt inhibitors (all non-toxic). The remaining 108 NEs were solely cytotoxic, with an IC$_{50}$ value ranging between 0.30 μg/mL and 50 μg/mL.

Out of these 241 inhibitory NEs, 132 NEs showed a Wnt-inhibition $IC_{50} < 50$ μg/mL, with 53 NEs having a Wnt-inhibition $IC_{50} < 10$ μg/mL. Focusing on samples capable of inhibiting the Wnt pathway is essential for discovering NPs to treat diseases linked to the dysregulation of this pathway. Therefore, in this study, only inhibitory NEs were further considered.

The 241 NEs with Wnt inhibitory activities mentioned above comprised a total of 58 different botanical families, 97 different genera, and 105 unique species. Fabaceae (Q44448) is the most represented family with 14 samples, followed by Rubiaceae (Q156569) and Euphorbiaceae (Q156584) with 9 and 8 samples respectively. The most represented genus is *Pandanus* (Q471914, Pandanaceae Q736182) with 5 samples, followed by *Sambucus* (Q131448, Adoxaceae Q156677) with 4 samples, and *Elegia* (Q3007993, Restionaceae Q131501), *Baliospermum* (Q4850999, Euphorbiaceae Q156584), and *Dolichos* (Q526727, Fabaceae), each with 3 samples.

To further reduce the list only NEs with an inhibition IC_{50} below 5 μg/mL were considered. This reduced the 241 to 30 NEs comprising 25 different species from 17 different botanical families, with Fabaceae and Euphorbiaceae being the most prominent, each contributing 5 NEs. Within this reduced set, there were 23 different genera, with the majority represented by only 1 NE, except for *Elegia* with 3 samples, and *Pandanus*, *Euphorbia* (Q146567), *Ehretia* (Q276756), and *Baliospermum* with 2 samples each.

The biological screening results drove the first selection step, resulting in a subset of 30 non-toxic NEs with an inhibitory $IC_{50} \leq 5$ μg/mL (see **Figure 1.A**). To further reduce this list, additional selection criteria based on UHPLC-HRMS[2] metabolite profiling data were used. In particular, *Inventa* scores for the potential structural novelty of metabolites (Quiros-Guerrero et al., 2022) present in active extracts were used.
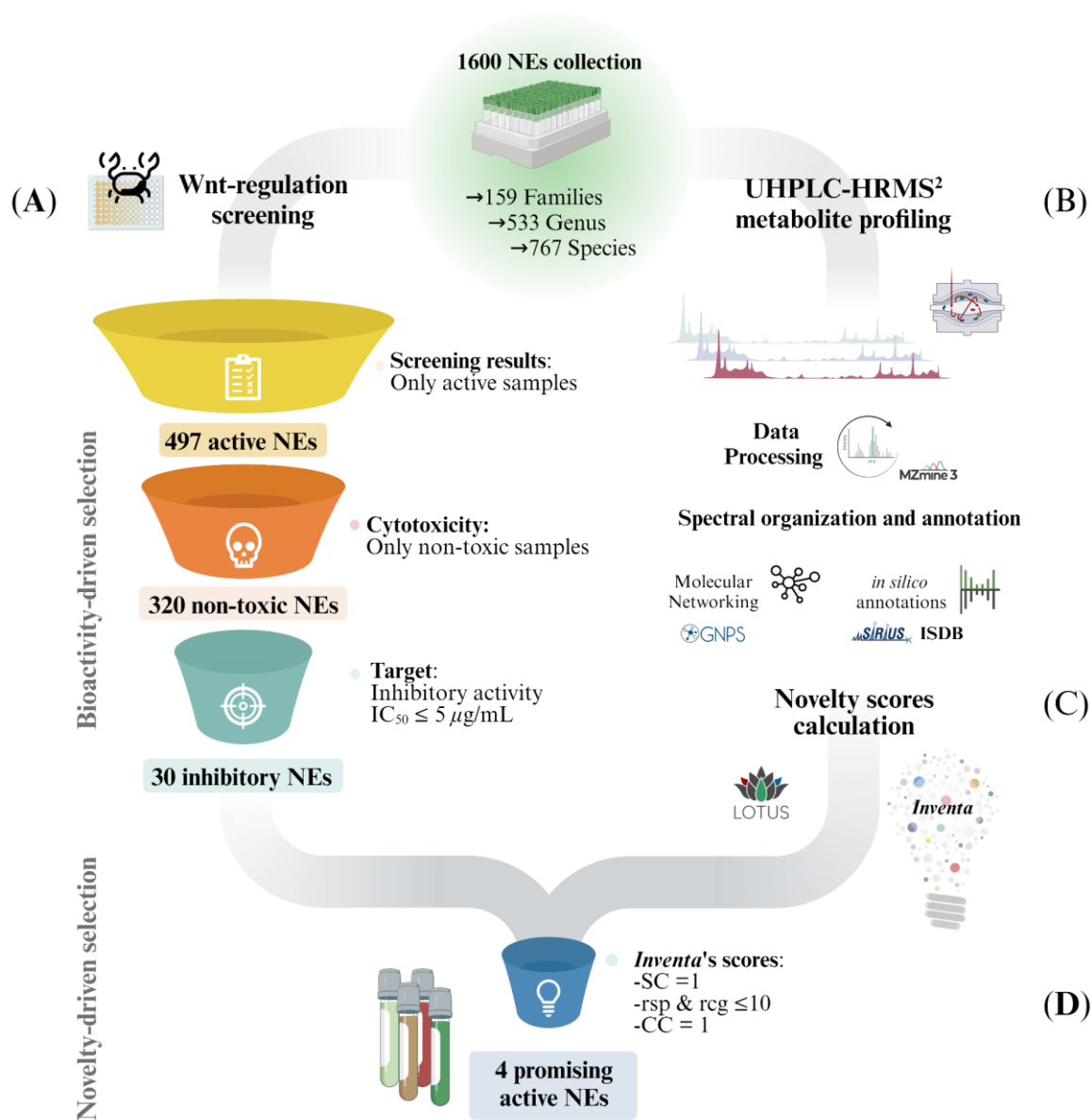
Figure 1. Overview of the general strategy for the selection of promising NEs for the discovery of structurally novel bioactive NPs in collections of NEs. (**A**) Bioactive-driven selection: The NEs collection is reduced according to the bioactivity screening results. In this study only non-toxic NEs with an Wnt inhibitory $IC_{50} \leq 5$ μg/mL were considered. (**B**) General overview of the UHPLC-HRMS^2 profiling and annotation workflow used for the characterization of the 1,600 NEs collection by Allard et al. (2023). (**C**) The UHPLC-HRMS^2 and annotations results for the entire 1,600 NEs collection were fed to *Inventa* to calculate the structural novelty scores. (**D**) Novelty-driven selection: Each component given by *Inventa* for the reduced set of NEs was individually assessed for a more precise selection. SC:

Similarity Component; CC: Class Component; rsp: reported compounds in species; rsg: reported compounds in genus.

Selection of promising NEs by combining bioactivity results and structural novelty scores.

Using the previous UHPLC-HRMS^2 metabolite profiling and dereplication results in the positive ionization (PI) mode (Allard et al., 2023) (**Figure 1.B**), *Inventa* (Quiros-Guerrero et al., 2022) was used to calculate the structural novelty scores for the entire 1,600 NEs set (**Figure 1.C**). In this study, the focus shifted from the entire collection of 1,600 NEs to a much smaller subset of 30 active NEs. Instead of selecting these NEs based on their overall PS assigned by *Inventa*, a more meticulous approach was adopted. Each *Inventa*'s component for these NEs was individually assessed for a more precise selection.

First, to ensure that only NEs potentially holding specific constituents (specific pool of MS^2 spectra), only those with a *Similarity Component* (SC) value of '1' were further considered. This score highlights extracts containing metabolites whose MS^2 spectra are significantly different from those of all 1,600 extracts in the data set. The SC employs the MEMO metric (Gaudry et al., 2022) to generate a matrix containing all MS^2 information in the form of peaks and neutral losses (Huber et al., 2020, 2021) and automatic outlier detection machine learning algorithms to emphasize NEs that display substantial spectral dissimilarity (Quiros-Guerrero et al., 2022). Out of the 30 NEs only 6 remained after this filter.

Then, only NEs with a *Literature Component* (LC) value close to '1' were selected. The value of LC reflects a rough estimation of the extent of the prior phytochemical knowledge for a given taxon (according to LOTUS). The closer to '1', the fewer compounds have been reported at the species, genus, and family levels for a given sample. *Inventa* calculates the number of reported compounds for each species, genus, and family, and this data forms part of the final information provided for each sample. Based on this information, only NEs reporting less than 10 reported compounds in both genus and species levels were further considered (**Figure 1.D**).

This reduced the 6 NEs to only 4 NEs with few compounds reported, since the species *Derris scandens* (Q15488445, Fabaceae) and *Iris lactea* (Q6747387, Iridaceae Q155941) presented over 100 and 400 compounds reported at the genus level respectively (see Wikidata Query results for genus *Derris* and *Iris*). Additionally, the remaining 4 NEs presented a *Class Component* (CC) of '1'. A CC value of 1 indicates that there are chemical classes proposed by CANOPUS (Dührkop et al., 2021) not yet reported for both the species and the genus (according to LOTUS). This suggests a high probability of potentially discovering unreported NPs within these NEs (Quiros-Guerrero et al. 2022).

The 4 highly active NEs remaining were: _Hymenocardia punctata_ Wall. ex Lindl. (Q15514019, Phyllanthaceae Q133206), _Aporosa villosa_ (Lindl.) Baill. (Q11128570, Euphorbiaceae Q156584), and 2 NEs of different plant parts of _Baliospermum sonalifolium_ (Burm.) Suresh (Q15386102, Euphorbiaceae).

To further refine the selection process, a thorough complementary literature search was done on this final set of three species, considering all the possible botanical synonyms according to WFO Plant List. This search revealed no direct reports for the _B. solanifolium_ species. However, for one of its synonyms, _B. montanum_ (Q3595677), the literature reports the presence of alkaloids, daphnanes, ingenanes, and phorbol esters (tiglianes Q27117179) like montanin (Q27107381) and baliospermin (Q27105913) (Seigler, 1994; Mali and Wadekar, 2008) with proven anticancer activity (Ogura et al., 1978). These metabolites were not accessible by Lotus, so they were not considered in first instance. Since _B. solanifolium_, presents active reported NPs, both extracts were no further considered. For _A. villosa_, some reports already described various bioactivities of ethanolic extracts from different plant parts were reported (Srikrishna et al., 2008; Venkataraman et al., 2010; Nanna et al., 2021). Additionally, preliminary metabolite profiling indicated a high concentration of fatty acids. Therefore, this plant was not initially considered for further study.

In contrast, for _H. punctata_, there were no existing reports on its chemical composition or bioactivity evaluation. This lack of information aligned with its initial _LC_ score based on the Lotus. Consequently, the ethyl acetate extract of _Hymenocardia punctata_ leaves was identified as the most promising candidate for the discovery of novel NPs. This plant is a flowering shrub from the Phyllanthaceae family, found in Myanmar, Thailand, Laos, Cambodia, the Malay Peninsula, and Sumatra (van Welzen, 2016).

Dereplication results overview for the ethyl acetate extract of _Hymenocardia punctata_ leaves.

According to _Inventa_'s results, the annotation rate for the _H. punctata_ extract was notably high (_c.a._ 75%). To further explore the regions of the chromatogram that were annotated, the comparison between the original (PI) UHPLC-HRMS^2 chromatogram (from the 1,600 NEs collection metabolite profiling) and the _Ionmap_ generated by _Inventa_ was carefully inspected (**Figure 2**). Upon examination of the SIRIUS and ISDB annotation results, as well as the outcomes of Ion Identity FBMN (II-FBMN, see **Supplementary Figure S1**, PDF version here) (Nothias et al., 2020; Schmid et al., 2021), it emerged clearly that the most intense features (**Figure 2.A**), were not annotated (green dots on the _Ionmap_ In **Figure 2.B**)
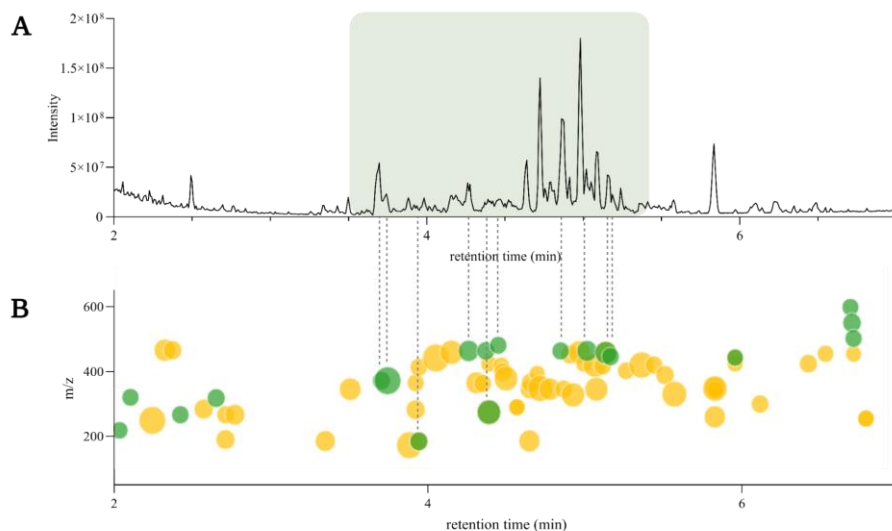
Figure 2. **A**) Original UHPLC-HRMS^2 chromatogram of *H. punctata* leaves ethyl acetate extract from the 1,600 NEs collection. **B**) *Inventa*'s ion map for the Original UHPLC-HRMS^2 chromatogram of *H. punctata* leaves ethyl acetate extract. Each dot represents one feature, the size is proportional to the intensity. The color shows the annotation status, green: unannotated, yellow: annotated (see interactive plot here).

For the subsequent phytochemical studies an ethyl acetate extract of the leaves of *H. punctata* was freshly prepared on a larger scale (HPE) and subjected to UHPLC-HRMS^2 metabolite profiling (HPE, **Figure 3.A**). For the HPE metabolite profiling a Charge Aerosol Detection (CAD) was used to obtain semiquantitative information (Ligor et al., 2013; Gamache, 2017) (**Figure 3.B**).

The (PI) UHPLC-HRMS^2 data from HPE was used to generate a new II-FBMN which confirmed most information obtained in the original extract from the 1,600 NEs collection. The most intense peaks were clustered together indicating their close structural relationship (II-FBMN, see **Supplementary Figure S2**, PDF version here). The chemical class and structural annotations obtained through GNPS, SIRIUS and CANOPUS (Dührkop et al., 2019, 2021) suggested that most compounds derived from the shikimate-phenylpropanoid and terpenoid pathways (refer to Treemap overview **Supplementary Figure S3** -interactive plot visualization here-, and **Supplementary Table SI**).

Both the CAD and MS traces confirmed that the major constituents of HPE were not annotated. This, together with the novelty scores given by *Inventa*, confirmed that HPE is a promising extract for the search for new bioactive NPs.
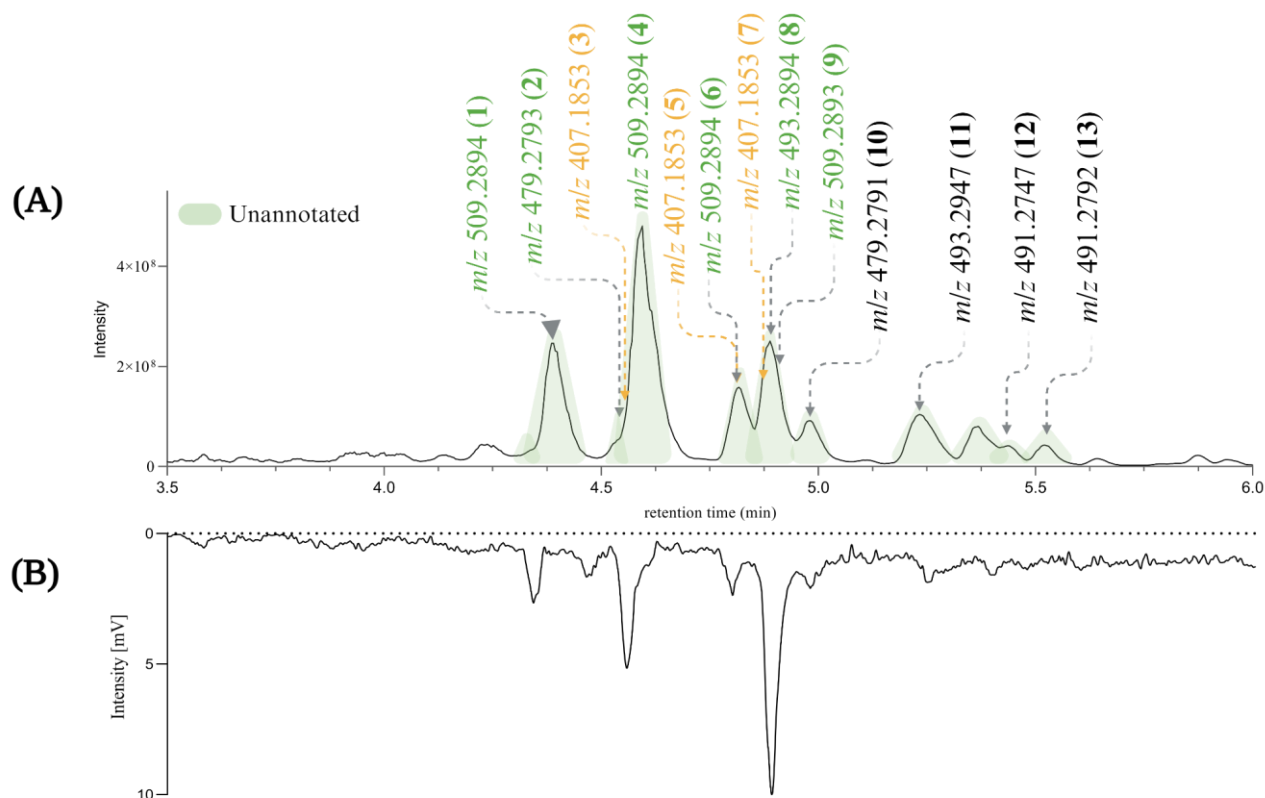
Figure 3. **A**) PI UHPLC-HRMS^2 chromatogram of *de novo H. punctata* leaves ethyl acetate extract (HPE) between 3.5 min and 6 min. **B**) Charge Aerosol Detector semiquantitative trace of HPE. The chromatographic peaks colored in green correspond to unannotated features after the dereplication process. The mass-to-charge ratio (*m/z*) of the most intense ions in the PI HRMS^2 trace are shown. The *m/z* colored in green (unannotated features) and yellow (annotated features) found in the original HRMS^2 profiling of *H. punctata* (in the 1,600 NEs collection, **Figure 2.A**).

HPLC-based bioactivity profiling of the ethyl acetate extract of *Hymenocardia punctata* leaves.

An HPLC-based bioactivity profiling (Hamburger, 2019) was carried out to establish a relationship between the major unannotated chromatographic peaks (potentially new NPs) and the observed bioactivity of HPE. A small amount of HPE (*c.a.* 10 mg) was fractionated by semi-preparative HPLC-UV under optimized chromatographic conditions. Column's effluent was collected into a 96 deep-well plate and the Wnt-regulatory bioactivity of each dried micro-fraction was assessed. The HPLC based bioactivity profile confirmed that the bioactivity was mainly related to the major unannotated peaks (See **Supplementary Figure S4**).

Isolation and *de novo* structural characterization of compounds from the *H. punctata* leaves ethyl acetate extract.

According to the dereplication results and the HPLC-based bioactivity profiling, the isolation efforts should be focused on the peaks with retention times between 3.5 and 6 minutes (see **Figure 3**). An in-depth phytochemical study of the HPE extract was carried out to corroborate the presence of structurally novel NPs and evaluate their Wnt regulatory activity. The chromatographic conditions used for the HPLC based bioactivity profiling were adapted to the flash chromatography scale using a geometrical gradient transfer (Guillarme et al., 2008). Several of the fractions obtained contained mixtures of compounds that were further separated by high resolution semi-preparative HPLC using dry-load injection (Queiroz et al., 2019).

This approach allowed the successful isolation of thirteen compounds (**1-13**, see **Figure 4**). The structures of all the compounds were determined based on the NMR and HRMS analyses. Three of these compounds were identified as 3′,8-diprenylapigenin (**3**) previously isolated from *Morus alba* (Q157307) (Dat et al., 2010), 6,8-diprenylapigenin (**5**) previously isolated from *Glycyrrhiza inflata* (Q5572787) (Lin et al., 2017), and 3′,6-diprenylapigenin (**7**) previously isolated from *Glycyrrhiza uralensis* (Q1196166) (Fukai et al., 1991). These compounds (**3**, **5**, **7**) were annotated as prenylated isoflavones by GNPS and Sirius. The other ten molecules corresponded to new compounds and were named *Hymenotamayonins* A-J (**1**, **2**, **4**, **6**, **8-13**), their full *de novo* structure identification is detailed below.

The relative retention time in the PI HRMS^2 chromatogram is depicted in **Figure 3** (numbers in parenthesis). The 13 compounds were recovered in sufficient amounts to allow full structural characterization and assessment of biological activity from only 55g of dried plant material.
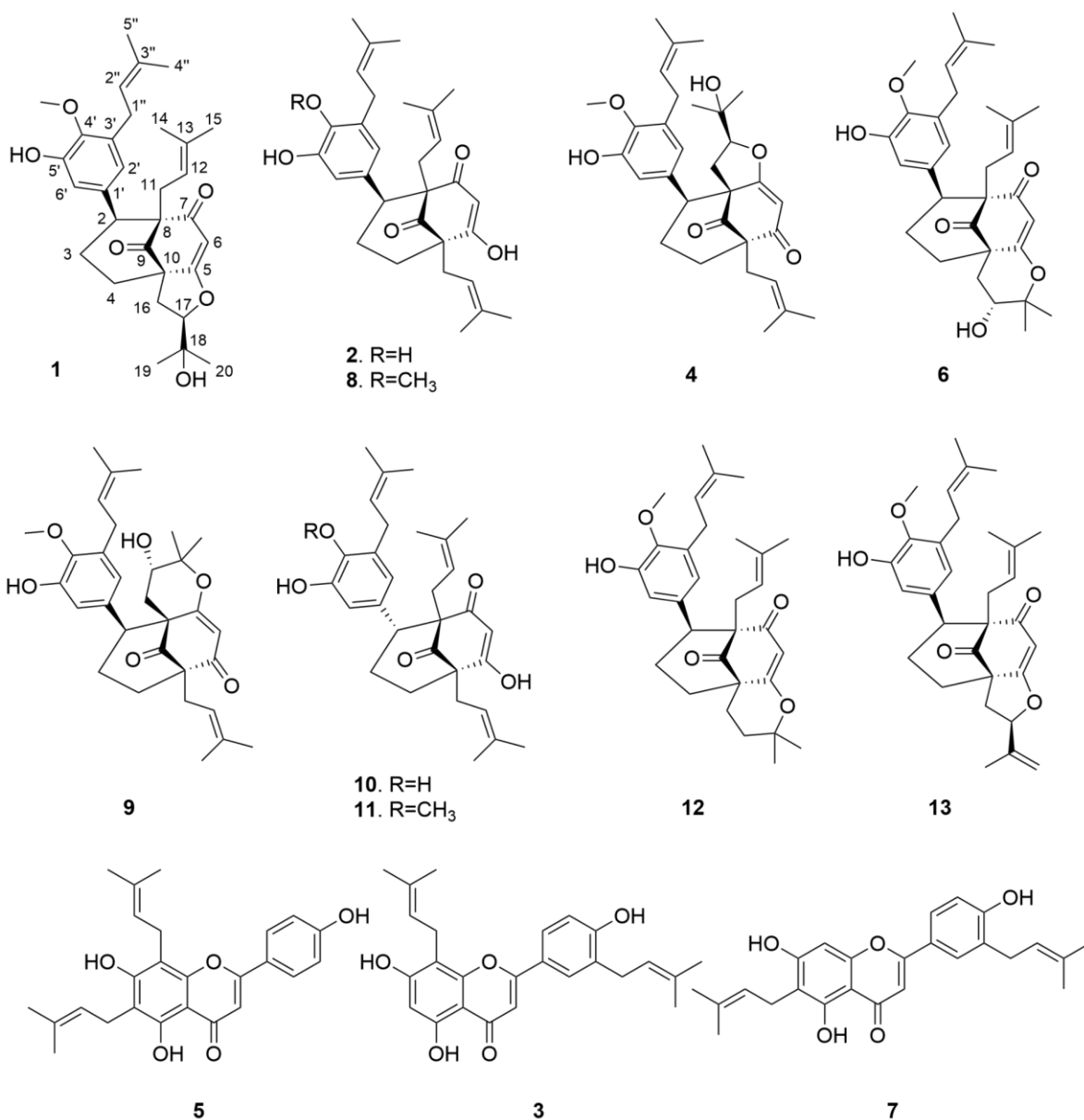
Figure 4. Structures of the isolated compounds from the ethyl acetate extract of *Hymenocardia punctata* leaves.

Compound **1** was isolated as an amorphous pale yellow powder with an $[M+H]^+$ of *m/z* 509.2894 corresponding to a molecular formula (MF) of $C_{31}H_{41}O_6$ (error -0.65 ppm). It corresponded to the peak at 4.4 min in **Figure 3**. The NMR data showed signals related to a 3-prenyl-4-methoxy-5-hydroxyphenyl group; with two meta aromatic protons coupled to each other ($J = 2.3$ Hz) at δ_H 6.38 (CH-2') and δ_H 6.47 (CH-6'), a methoxy singlet at δ_H 3.75 (4'-OCH$_3$), a methylene at δ_H 3.28 (2H, m, CH$_2$-1"), a vinylic proton at δ_H 5.24 (1H, thept, $J = 6.7, 1.3$ Hz, CH-2") and two methyl groups at δ_H 1.73 (3H, d, $J = 1.3$ Hz, CH$_3$-4") and δ_H 1.77 (3H, d, $J = 1.3$ Hz, CH$_3$-5"). This part of the molecule

was confirmed based on the HMBC correlations from CH-2' to C-1" (δ_C 29.1), C-4' (δ_C 146.0), and C-6' (δ_C 115.8), from H-6' to C-2' (δ_C 121.6), C-4' and C-5' (δ_C 151.0), from CH$_3$-4" and CH$_3$-5" to C-3" (δ_C 133.6) and C-2" (δ_C 123.9), from CH$_2$-1" to C-2', C-3' (δ_C 136.3), C-4', C-2" and C-3", and from 4'-OCH$_3$ to C-4' (see **Figure 5**). A second prenyl group was identified based on the signals at δ_H 2.05 and δ_H 2.17 for the methylene CH$_2$-11, δ_H 4.76 for the ethylenic proton CH-12, and δ_H 1.48 and δ_H 1.50 for the two methyl groups CH$_3$-14 and CH$_3$-15. The COSY correlation from the methylene CH$_2$-16 (δ_H 1.91 and δ_H 2.82) to the oxymethine CH-17 (δ_H 4.72) and the HMBC correlations from the methyl groups CH$_3$-19 and CH$_3$-20 (δ_H 1.21 and δ_H 1.34) to C-18 (δ_C 71.1) and CH-17 (δ_C 92.8) allowed the identification of a 3-methylbutyl chain with positions 2 and 3 oxygenated. The aromatic moiety from the 3-prenyl-4-methoxy-5-hydroxyphenyl group was shown to be linked to a methine, which is connected to two consecutive methylenes. This was evidence thanks to the HMBC correlations from the methine CH-2 (δ_H 3.12) to C-1' (δ_C 137.9), C-2', C-6', the methylenes CH$_2$-3 (δ_C 27.5) and CH$_2$-4 (δ_C 33.1), as well as the one from CH-3$_{eq}$ (δ_H 1.64) to C-1' (see **Figure 5**). A vinylic singlet at δ_H 5.80 (CH-6), two quaternary carbons (δ_C 61.7 (C-10) and 67.2 (C-8)), and three carbonyl carbons (δ_C 181.2 (C-5), 201.3 (C-7), and 207.7 (C-9)) fitted the number of carbons (31) with the molecular formula. The HMBC correlations from CH$_2$-11 to CH-2, C-7, C-8, and C-9, from CH$_2$-16 to CH$_2$-4, C-5, C-9, and C-10, from CH-6 to C-5, C-8, and C-10, from CH-2 to C-7, and C-9, and from CH$_2$-4 to C-5 allowed to position the 3-prenyl-4-methoxy-5-hydroxyphenyl group, the prenyl, and the 2,3-dihydroxy-3-methylbutyl group on a bicyclic[3.3.1] core as shown in **Figure 4**. The carbons C-8 and C-10 are bridged by a ketone (C-9) with a typical chemical shift (δ_C 207.7). These carbons together with CH-2, CH$_2$-3, and CH$_2$-4 integrate the first 6-member ring. The second ring shares the carbons C-8, C-9, and C-10 with a keto-enol system between carbons C-5, C-6, and C-7. According to the molecular formula, an additional ring must be established either between the tertiary alcohol in C-18 and C-5 to form a tetrahydropyran ring, or between the secondary alcohol in C-17 and C-5 to form a tetrahydrofuran ring. The lack of HMBC correlation between CH-17 and C-5 could not answer this question. Measurements in CDCl$_3$ were done to try to find correlations between these protons by avoiding solvent exchanges, but they did not show any correlations either. However, the CH-17 and C-18 chemical shift values (δ_C 92.8 and δ_C 71.1, respectively) compared to values in the literature for oblongifolin R (which presents a tetrahydrofuran ring with CH at δ_C 94.8 and C at δ_C 71.1) and oblongifolin S (bearing a tetrahydropyran ring with CH at δ_C 69.6 and C at δ_C 86.9) (Zhang et al., 2014) led to the conclusion that a 5-member ring is present. The two-dimensional structure of compound **1** was established as shown in **Figure 4**. The relative configuration was established through the ROESY correlations observed in CD$_3$OD and CDCl$_3$. The spectra recorded in CDCl$_3$ helped identify the pseudo equatorial

and axial positions of CH$_2$-3 and CH$_2$-4 protons. These proton signals overlapped with other ones in CD$_3$OD. The ROESY correlations from CH-2'/CH-6' to CH-4$_{ax}$ indicated that the 3-prenyl-4-methoxy-5-hydroxyphenyl group was in a pseudo axial position and the coupling constant value of CH-2 ($J =$ 5.4 Hz in CD$_3$OD, $J = 6.1$ Hz in CDCl$_3$) confirmed that CH-2 was in a pseudo equatorial position (**Figure 6.A**). The correlation between CH-17 and CH-4$_{eq}$ indicated the relative configuration of C-17 (**Figure 6.A**). Consequently, the relative configuration of **1** was proposed as (2*S*,8*R*,10*R*,17*R*) or (2*R*,8*S*,10*S*,17*S*). To establish its absolute configuration, the ECD spectrum was calculated based on the relative configuration proposed by NMR and compared to the experimental data (**Figure 6.B**). Thus, compound **1** was assigned as (2*S*,8*R*,10*R*,17*R*)-2-(5-hydroxy, 4-methoxy-3-(3-methylbut-2-en-1-yl)phenyl)-12-(2-hydroxypropan-2-yl)-8-(3-methylbut-2-en-1-yl)-5-oxotricyclo[6.3.1.0^{5,10}]dodec-5-ene-7,9-dione and named Hymenotamayonin G.
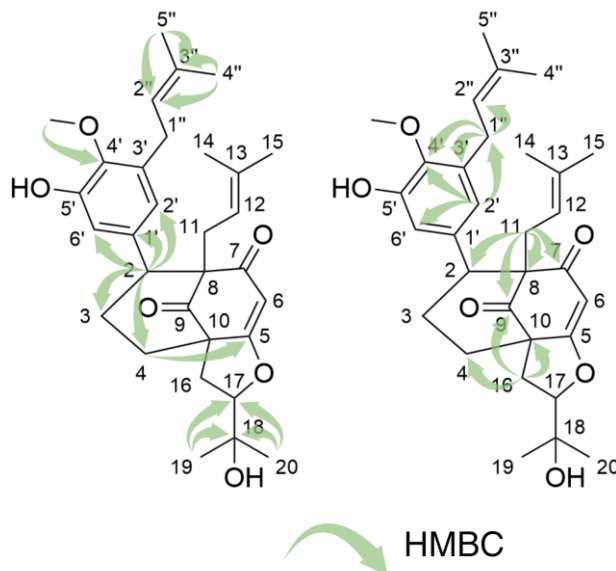
Figure 5. Key HMBC correlation for compound **1**.
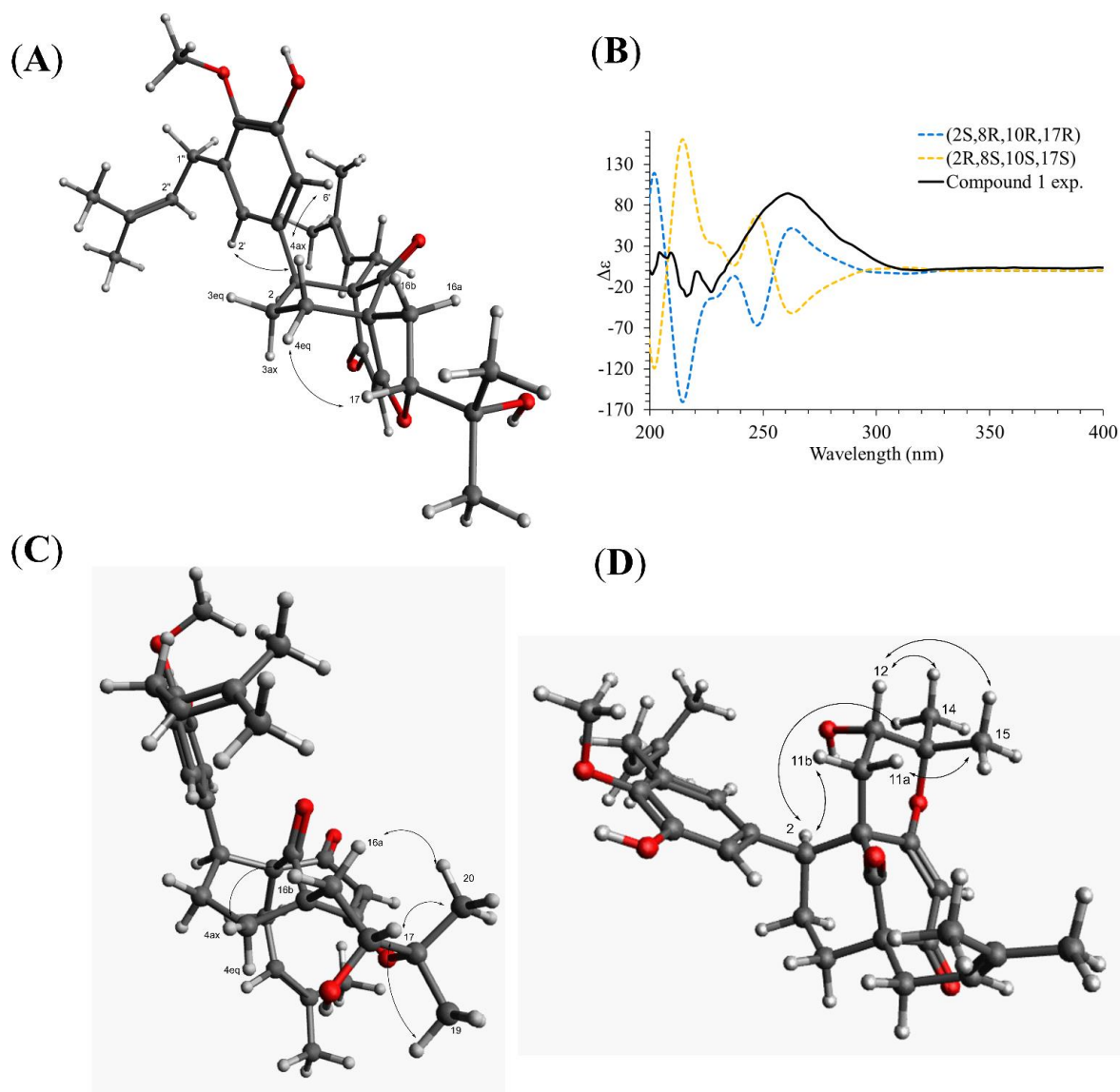
Figure 6. (**A**) Key dipolar correlations and ROESY spectrum for compound **1**. (**B**) Experimental and B3LYP/def2svp//B3LYP/6-31G(d,p) calculated ECD spectra in methanol for compound **1**. (**C**) Key dipolar correlations for compound **6**. (**D**) Key dipolar correlations for compound **9**.

Compound **2** was isolated as an amorphous pale yellow powder with an [M+H]$^+$ of m/z 479.2793 corresponding to MF of $C_{30}H_{39}O_5$ (error 0.21 ppm). It corresponded to the peak at 4.5 min in **Figure 3**. The ^{1}H NMR data compared to that of **1** showed that: i) the vinylic singlet at δ_H 5.80 (CH-6) was missing, ii) the methoxy (4'-OCH$_3$) signal was absent, and iii) signals from the 2,3-dihydroxy-

3-methylbutyl chain were replaced by those belonging to a third prenyl group (a methylene CH_2-16 at δ_H 2.47/2.57, a vinylic proton CH-17 at δ_H 5.19, and two methyl CH_3-20/CH_3-19 δ_H 1.68/1.70). This prenyl group was positioned in C-10 thanks to the HMBC correlations from CH_2-16 to the methylene CH_2-4 (δ_C 34.7), the quaternary carbon C-10 (δ_C 61.6) and the ketone C-9 (δ_C 211.9). To fit with the molecular formula, an enolized 1,3-diketone was placed in C-5, C-6, and C-7. Due to the rapid tautomeric equilibrium and H/D exchange with the solvent, the ^{1}H and ^{13}C signals of C-5, CH-6, and C-7 were not observed (Traven et al., 1997; Rajaonarivelo et al., 2016) (See **Supplementary Figure S5**). The relative configuration of **2** was the same as described for **1**, and the absolute configuration was confirmed with the comparison between the calculated and experimental ECD spectra (See **Supplementary Figure S6**). Thus compound **2** was identified as (2*S*,8*R*,10*R*)-(4,5-dihydroxy-3-(3-methylbut-2-en-1-yl)phenyl)-5-hydroxy-8,10-bis(3-methylbut-2-en-1-yl)bicyclo[3.3.1]non-6-ene-7,9-dione and named Hymenotamayonin A.

The molecular weight of compound **4**, *m/z* 509.2894 [M+H]$^+$ (calculated for MF $C_{31}H_{41}O_6$, error -0.65 ppm) was the same as compound **1** and the NMR data were also very close with the same functional groups: a 3-prenyl-4-methoxy-5-hydroxyphenyl, a prenyl group, a 2,3-dihydroxy-3-methylbutyl chain, all attached to a bicyclic[3.3.1] core. The difference between **1** and **4** was the positions of the prenyl group and the 2,3-dihydroxy-3-methylbutyl chain in the bicyclic core. In **4**, the HMBC correlations from the methylene CH_2-16 of the prenyl at δ_H 2.43/2.53 to CH_2-4 (δ_C 27.8), C-10 (δ_C 64.4), C-5 (δ_C 200.7), and C-9 (δ_C 208.0), and from the methylene CH_2-11 of the 2,3-dihydroxy-3-methylbutyl chain at δ_H 1.74/2.53 to CH-2 (δ_C 49.4), C-8 (δ_C 64.7), and C-7 (δ_C 182.1) indicated that the prenyl was in C-10 and the 2,3-dihydroxy-3-methylbutyl chain was in C-8. As in **1**, the chemical shift of CH-12 (δ_C 92.2) and C-13 (δ_C 71.1) showed that a tetrahydrofuran ring is present between CH-12 and C-7. The coupling constant of CH-2 (d, *J* = 6.4 Hz) and the ROESY from the aromatic protons CH-2' and CH-6' to CH-4ax at δ_H 2.08 (td, *J* = 14.1, 4.8 Hz) indicated that as in **1**, that the aromatic group is in a pseudo axial configuration. The ROESY correlation from CH-2 to the methine CH-12 of the tetrahydrofuran group showed that the configuration of C-12 and C-2 is *S*. Comparison of the experimental and calculated ECD spectra corroborated this observation (See **Supplementary Figure S6**). Compound **4** was identified as (2*S*,8*R*,10*R*,12*S*)-2-(5-hydroxy, 4-methoxy-3-(3-methylbut-2-en-1-yl)phenyl)-17-(2-hydroxypropan-2-yl)-10-(3-methylbut-2-en-1-yl-7-oxotricyclo[6.3.1.0$^{7,8}$]dodec-6-ene-5,9-dione and named Hymenotamayonin H. It corresponded to one of the major peak at 4.6 min in both, MS and CAD traces (**Figure 3**).

Similar to **1**, compound **6** exhibited an MF of $C_{31}H_{40}O_6$ (*m/z* 509.2894 [M+H]$^+$, error -0.65 ppm). The NMR data of **6** were very close to those of **1** and indicated that the connectivity and configuration of the bicyclic[3.3.1] core, the pseudo axial position of the 3-prenyl-4-methoxy-5-hydroxyphenyl group in C-2, the linkage of the prenyl group in C-8 were the same as those described for **1**. The main differences concerned the 2,3-dihydroxy-3-methylbutyl chain for which the chemical shift values of the oxymethine C-17 were observed at δ_C 69.9 (δ_C 92.8 for **1**) and the quaternary oxygenated carbon C-18 at δ_C 84.8 (δ_C 71.1 for **1**). This agreed with the presence of a tetrahydropyran ring (**Figure 4**). The configuration at C-17 was determined thanks to the ROESY correlation from CH-16eq at δ_H 1.74 (dd, *J* = 14.9, 5.3 Hz) to CH-4ax at δ_H 2.09 (td, *J* = 14.5, 4.6 Hz), from CH-16ax at δ_H 2.94 (dd, *J* = 14.9, 3.9 Hz) to CH$_3$-20 at δ_H 1.26 (**Figure 6.C**). The coupling constant value of CH-17 (t, *J* = 5.3, 3.9 Hz) and its ROESY correlations with CH$_3$-19 and CH$_3$-20 indicated its equatorial position. The configuration proposed was confirmed by comparison of the experimental and calculated ECD spectra (See **Supplementary Figure S6**). Compound **6** was then identified as (2*S*,8*R*,10*R*,17*R*)-17-hydroxy-2-(5-hydroxy, 4-methoxy-3-(3-methylbut-2-en-1-yl)phenyl)-18,18-dimethyl-8-(3-methylbut-2-en-1-yl)-5-oxotricyclo[7.3.1.0^{5,10}]dodec-5-ene-7,9-dione and named Hymenotamayonin I. It corresponded to one of the peaks at 4.8 min in **Figure 3**.

The HRMS and NMR data showed that compound **8** (Hymenotamayonin C) was the *O*-methyl derivative of **2**: (2*S*,8*R*,10*R*)-2-(5-hydroxy-4-methoxy-3-(3-methylbut-2-en-1-yl)phenyl)-5-hydroxy-8,10-bis(3-methylbut-2-en-1-yl)bicyclo[3.3.1]non-6-ene-7,9-dione. Thus, the group in C-2 was the same as **1**, **4,** and **6**: a 3-prenyl-4-methoxy-5-hydroxyphenyl group. It corresponded to one of the peaks at 4.9 min in **Figure 3**.

The NMR data of **9** displayed very close similarities to those of **4**, for the same MF as indicated by the HRMS ion at *m/z* 509.2893 [M+H]$^+$. As for the previous comparison between **6** and **1**, the difference between **9** and **4** was the presence of a tetrahydropyran ring in **9** whereas **4** had a tetrahydrofuran ring in the same place. This was indicated by the chemical shift's values of CH-12 (δ_C 70.5) and C-13 (δ_C 85.3), in **9** compared to those of **4** (δ_C 92.2 and δ_C 71.1, respectively). The ROESY from CH-11eq at δ_H 1.59 (dd, *J* = 14.7, 7.8 Hz) to CH-2 at δ_H 3.63 (d, *J* = 6.2 Hz), from CH-11ax at δ_H 2.61 (dd, *J* = 14.7, 3.9 Hz) to CH$_3$-15 at δ_H 1.26 indicated the *S* configuration at C-12 (See **Figure 6.D**). Thus, compound **9** was identified as (2*S*,8*R*,10*R*,12*S*)-12-hydroxy-2-(5-hydroxy, 4-methoxy-3-(3-methylbut-2-en-1-yl)phenyl)-13,13-dimethyl-10-(3-methylbut-2-en-1-yl)-7-oxotricyclo[7.3.1.0^{7,8}]dodec-5-ene-5,9-dione and named Hymenotamayonin J. Its absolute configuration was confirmed based on the comparison of the experimental and calculated ECD spectra (See **Supplementary Figure S6**).

The NMR data of **10** were closely related to those of **2** and the HRMS data confirmed that both molecules had the same MF $C_{30}H_{39}O_5$ (*m/z* 479.2791 [M+H]$^+$, error -0.19 ppm). The main differences were the chemical shift value of CH-2 and its coupling constants. Whereas the chemical shift values of CH-2 were observed above δ_H 3.00 in the previous compounds it appeared shielded in **10** at δ_H 2.64. In the previous compounds, CH-2 was observed as a doublet with a coupling constant between 5.4 Hz and 6.4 Hz. In **10**, CH-2 resonated as a doublet of doublet (*J* = 13.2, 4.0 Hz) indicating that it was, in a pseudo-axial configuration. This was confirmed by the ROESY correlation from CH-2 to CH-4ax at δ_H 1.64 (overlapped). Thus, compound **10** was identified as (2*R*,8*R*,10*R*)-2-(4,5-dihydroxy-3-(3-methylbut-2-en-1-yl)phenyl)-5-hydroxy-8,10-bis(3-methylbut-2-en-1-yl)bicyclo[3.3.1]non-6-ene-7,9-dione and named Hymenotamayonin B. It corresponded to one of the peaks at 4.95 min in **Figure 3**.

The NMR and HRMS data of **11** indicated that it was the 4'-*O*-methyl derivative of **10**, thus (2*R*,8*R*,10*R*)-2-(5-hydroxy-4-methoxy-3-(3-methylbut-2-en-1-yl)phenyl)-5-hydroxy-8,10-bis(3-methylbut-2-en-1-yl)bicyclo[3.3.1]non-6-ene-7,9-dione (Hymenotamayonin D). It corresponded to one of the peaks at 5.25 min in **Figure 3**. The HRMS of **12** gave an [M+H]$^+$ at *m/z* 493.2747 calculated for an MF $C_{31}H_{41}O_5$ (error -0.16 ppm). The NMR data showed as in **6**, that the bicyclic[3.3.1] core presented a 3-prenyl-4-methoxy-5-hydroxyphenyl substitution in a pseudo axial configuration in C-2 and a prenyl group in C-8. The oxymethine CH-17 observed in the tetrahydropyran ring of **6** was replaced by a methylene (δ_H 2.04 (td, *J* = 14.3, 4.1 Hz, CH-17ax), δ_H 1.86 (dt, *J* = 14.3, 4.1 Hz, CH-17eq) and δ_C 31.2). The HMBC correlations from CH-16ax (δ_H 2.56, td, *J* = 14.4, 4.2 Hz) to CH$_2$-4 (δ_C 33.2) and C-10 (δ_C 51.0), from CH-17eq to C-10, from CH-16eq (δ_H 1.71, dt, *J* = 14.4, 4.2 Hz), CH$_3$-19 (δ_H 1.46) and CH$_3$-20 (δ_H 1.29) to quaternary oxygenated carbon C-18 (δ_C 82.3) confirmed that **12** was the 17-deoxy derivative of **6**: (2*S*,8*R*,10*R*)-2-(5-hydroxy, 4-methoxy-3-(3-methylbut-2-en-1-yl)phenyl)-18,18-dimethyl-8-(3-methylbut-2-en-1-yl)-5-oxotricyclo[7.3.1.0^{5,10}]dodec-5-ene-7,9-dione (Hymenotamayonin F). It corresponded to one of the peaks at 5.45 min in **Figure 3**.

The MF of **13** was established as $C_{31}H_{38}O_5$ by HRMS (*m/z* 491.2792 [M+H]$^+$, error 0.08 ppm). As compounds **1**, **6**, **8**, **11,** and **12**, the NMR data of **13** showed signals corresponding to a bicyclic[3.3.1] core with, in C-2, a 3-prenyl-4-methoxy-5-hydroxyphenyl in a pseudo axial configuration and, in C-8, a prenyl group. Similar to **1**, a tetrahydrofuran ring was observed between C-10 and C-5, as indicated by the signals from the methylene CH$_2$-16 (δ_H 2.63/δ_H 2.12) and the oxymethine CH-17 (δ_H 5.32). The HMBC correlations from the methylidene observed at δ_H 5.17 (q, *J* = 1.2 Hz, CH-20a) and δ_H 5.05 (p, *J* = 1.2 Hz, CH-20b) to the oxymethine CH-17 (δ_C 89.2), the vinylic carbon C-18 (δ_C 143.1) and the methyl CH$_3$-19 (δ_C 17.3) enabled the identification of the structure

shown in **Figure 4**. The configuration in C-17 was determined as R thanks to the ROESY correlations from CH-17 to CH-4eq (δ_H 2.23, brd, J = 9.4 Hz, the relative configuration of the other carbons were established as (2S,8R,10R). Thus, compound **13** was identified as (2S,8R,10R,17R)-2-(5-hydroxy, 4-methoxy-3-(3-methylbut-2-en-1-yl)phenyl)-8-(3-methylbut-2-en-1-yl)-17-(prop-1-en-2-yl-5-oxotricyclo[6.3.1.0^{5,10}]dodec-5-ene-7,9-dione and named as Hymenotamayonin E. It corresponded to one of the peaks at 5.5 min in **Figure 3**.

Compounds **1,2,4,6**, and **8**-**13** make part of a very restricted group of NPs that contain an uncommon bicyclo[3.3.1]non-3-ene-2,9-dione core (Lin et al., 2018). To date, only three NPs with this core have been reported. The first compound ever reported in this class was acutifolin A (Q15410235), isolated from a Moraceae (Q156579) Brazilian medicinal plant *Brosimum acutifolium* (Q15471077) (Takashima and Ohsaki, 2001). Later, tazettone A and tazettone B were isolated from *Narcissus tazetta* var. *chinensis* (Q25115128) (Fu et al., 2013), an Amaryllidaceae (Q155848). According to the Angiosperm (Q14832431) phylogeny grouping, *N. tazzeta* belongs to the Asparagales order (Q26229), while *B. acutifolium* and *H. punctata* are comprised in the Fabids clade (Q2683213) but in different orders, Rosales (Q21895) and Malpighiales (Q21887), respectively. There are therefore no closer taxonomic relationships between these species that could explain common biosynthetic pathways (The Angiosperm Phylogeny Group, 2009).

From a biosynthetic point of view, the new compounds isolated from *H. punctata* may have been formed by rearrangement of an 8-prenylflavane as suggested for acutifolin A, tazettone A, and tazettone B (**Figure 7**). A similar rearrangement occurs also when catechin is subjected to basic conditions, forming catechinic acid (Sears et al., 1974; Ibrahim et al., 2007; Khiari et al., 2017). The extraction process was under neutral conditions, which is an indication of the authenticity of the compounds. The proposed biosynthesis pathway involves the presence of an electrophilic species that introduces the hydroxy group at position C-10 in acutifolin A, and tazettone A and B. We hypothesize that, in our case, this electrophilic species is a dimethylallyl diphosphate (DMAPP) unit, resulting in the prenylation of the position C-10 (Yazaki et al., 2009; Zhou et al., 2021). This assertion is plausible since we were able to isolate prenylated flavonoids (**3**, **5** and **7**), which is an indication of their abundance in this plant.
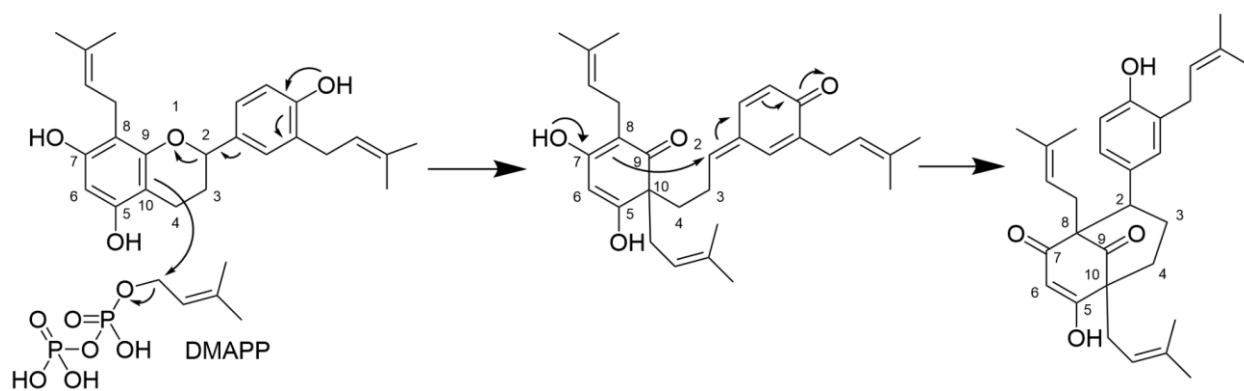
Figure 7. Proposed biosynthesis for the bicyclo[3.3.1]non-3-ene-2,9-dione core of compounds **1**,**2**,**4**,**6**, and **8**-**13**.

Evaluation of the Wnt-regulatory activity of isolated compounds.

The Wnt-regulatory activity of all isolated compounds from *H. punctata* was evaluated using two different cancer cell lines representing TNB cancer, known for its reliance on Wnt signaling: BT-20 and HCC1395 cells. Additionally, Human Embryonic Kidney HEK293 cells were used to represent non-malignant cells. The results for the active compounds are shown in **Table 3** (and **Supplementary Figure S7**).

The results demonstrated that the prenylated flavone **7**, exhibited the highest potency against the HEK293 cell line, with an IC_{50} value of 12 μM. Other compounds exhibited significantly higher selectivity against HCC1395 cancer cells. For example, the other prenylated flavone **3** demonstrated the highest selectivity, followed by one of the newly discovered bicyclic compounds **4,** with IC_{50} values of 13 μM and 14 μM, respectively. Notably, their potency against both BT-20 and HEK293 cells was nearly two-fold lower. In the case of the BT-20 cell line, **7** displayed the highest activity, followed by **4**, with IC_{50} values of 16 μM and 26 μM, respectively. It is worth noting that, in general, the prenylated flavones (**3** and **7**) had lower IC_{50} values compared to the novel bicyclic compounds (**1**, **2** and **4**) in at least two out of the three different cell models. Additionally, for all compounds, the specificity for Wnt inhibition was controlled by the absence of effects of the compounds on co-transfected constitutively expressed Renilla luciferase, serving as a reporter of cytotoxic or other negative effects of the compounds on the cell well-being (Shaw et al., 2019a).

Over the past two decades, numerous studies have revealed that flavonoids and structurally related compounds possess inhibitory effects on human diseases by targeting various cellular signaling components (Amado et al., 2011, 2014). Flavonoids have been recognized as inhibitors of the Wnt pathway, with many of them shown to inhibit it by downregulating the levels of *β*-catenin (Fuentes et

al., 2015). For instance, Apigenin (Q424567), the first flavonoid to be reported as a Wnt inhibitor, has been found to decrease β-catenin levels and promote cell cycle arrest in breast and colorectal cancer (Song et al., 2000; Landesman-Bollag et al., 2001; Amado et al., 2011). However, to date, there have been no reported findings of whether and how prenylation changes the potency of flavones towards the Wnt/β-catenin pathway. A few reports show the direct activity of prenylated isoflavones, such as 8-prenylgenistein by promoting osteogenesis (Zhang et al., 2018; Qiu et al., 2020). Our results clearly demonstrate that prenylated flavones, and similar analogs like the new bicyclic compounds, selectively disrupt the Wnt/β-catenin pathway, however with a potency only modestly improved from that reported for apigenin, from *c.a.* 30 μM down to 10-20 μM. This is also paralleled by other studies showing that structurally similar prenylated chalcones such as derricin and derricidin isolated from *Lonchocarpus sericeus* (Q15471182) reduce cell viability and induce cell cycle arrest in colorectal cancer HCT116 cells (Q28334584) through negative modulation of the Wnt/β-catenin pathway (Stevens, 2020).

Experimental Section

General Experimental Procedures.

The plant material was extracted in a Thermo Scientific Dionex ASE 350 Accelerated Solvent Extractor (Thermo Scientific™, Bremen, Germany). HPLC analyses were performed on an HP 1260 Infinity Agilent High-Performance Liquid Chromatography System equipped with a photodiode array detector (HPLC-PDA) (Agilent Technologies, Santa Clara, CA, United States) connected to an Evaporative Light Scattering Detector (ELSD, SEDERE, Orleans, France). The HPLC-based biactivity profiling was performed on an HP 1260 Agilent Infinity II High-Performance liquid chromatography equipped with a photodiode array detector (HPLC-PDA) and a sample collector (Agilent Technologies, Santa Clara, CA, United States). Flash chromatography was performed on a Sepacore instrument (Buchi, Flawil, Switzerland) composed of a pump module C-605, fraction collector model C-620, and UV spectrophotometer model C-640. The semi-preparative HPLC was performed using a Shimadzu system consisting of LC-20A module pumps, an SPD-20A UV/Vis detector, a 7725I Rheodyne® valve, and an FRC-10A fraction collector (Shimadzu, Kyoto, Japan). The system was controlled using the LabSolutions software from Shimadzu. NMR spectroscopic data were acquired on a Bruker Avance Neo 600 MHz spectrometer equipped with a QCI 5 mm Cryoprobe and a sampleJet automated extract changer (Bruker BioSpin, Rheinstetten, Germany). Chemical shifts are reported in parts per million (ppm, δ), and coupling constants are reported in Hertz (Hz, *J)*. The residual CD_3OD / $CDCl_3$ signals (δ_H 3.31/7.26, δ_C 49.8/77.16) were used as internal standards for ^{1}H and ^{13}C, respectively.

Comprehensive assignments were based on 2D-NMR spectroscopy techniques such as COSY, edited-HSQC, HMBC, and ROESY. Electronic Circular Dichroism (ECD) measurements were measured using a JASCO J-815 spectrometer (Loveland, CO, United States) in methanol, utilizing a 1 cm cell. The scan speed was set at 200 nm/min in continuous mode, scanning from 400 nm to 165 nm. Optical rotations were determined in methanol using a JASCO P-1030 polarimeter (Loveland, CO, USA) with a 1 mL, 10 cm tube.

Extraction of plant material.

PFL supplied the dried, grounded leaves of *Hymenocardia punctata* (Phyllanthaceae) (identifier V114372GP-01). This plant was part of the PFL collection registered with the European Commission on April 1, 2020, under accession number 03-FR-2020. This official registration acknowledges the collection's compliance with legal standards for access and management. It signifies that the PFL collection adheres to the European Access and Benefit Sharing Regulation criteria, which enforces the Nagoya Protocol's directives at the European level. These directives pertain to accessing genetic resources and justly sharing the benefits derived from their use.

A mass of 55 g was extracted in a 100 mL pressure-resistant stainless steel extraction cell using an ASE system. At the bottom and the top of the cell, a cellulose filter (Dionex™ 100, Thermo Scientific™, Bremen, Germany) was added to prevent solid particles from reaching the internal system. The cell was extracted with 60% rinse volume under pressure at 40°C, 3 cycles, and a static time of 5 min per cycle. The sample was extracted successively with HPLC quality hexane (Fisher Chemicals, Reinach, Switzerland), ethyl acetate (Fisher Chemicals, Reinach, Switzerland), and methanol (Fisher Chemicals, Reinach, Switzerland). The resulting extracts were dried at 35°C under vacuum in a rotary evaporator to yield 0.32 g of hexanic extract (HPH), 1.13 g of ethyl acetate extract (HPE), and 2.60 g of methanolic extract (HPM).

HPLC-based fractioning of HPE extract for bioactivity profiling.

A mass of 10 mg of HPE was dissolved in 200 μL of DMSO (molecular biology grade, Sigma, St Louis, United States) and then separated on an X-Bridge C_{18} column (250×10 mm i.d., 5 μm) equipped with a Waters C_{18} precolumn cartridge holder (5×10 mm i.d., 5 μm). The flow rate was set to 3.700 mL/min, and a binary solvent system consisting of 0.1% aqueous formic acid [A] and 0.1% formic acid in ACN [B] (Fisher Chemicals, Reinach, Switzerland) was used. A gradient (v/v) of [B] was employed as follows [t(min), %B]: 0.00, 2; 2.00, 2; 6.00, 50; 30.00, 100; 34.0, 100; followed by re-equilibration steps (36.00, 2; 40.00, 2). The collection was done at a fixed fraction volume of 1.600 mL per well (96-W 2 mL Deep Well Plate, Scientific Specialties Inc., California, USA). A 100

μL aliquot of each well was pooled (row-wise and column-wise) in a preweighted vial and then dried under an N_2 flux. After weighing, each pooled-sample was reconstituted in DMSO at 5 mg/mL.

Isolation of compounds from the HPE Extract.

The HPE (1.1 g) was separated on a Puriflash C18-HP column (200 x 30 mm I.D., 15 μm, Interchim, Montlucon, France) on a Buchi system. The flow rate was set to 60 mL/min, and a binary solvent system consisting of 0.1% aqueous formic acid [A] and 0.1% formic acid in acetonitrile [B] was used. A gradient (v/v) of [B] was employed as follows [t(min), %B]: 0.00, 2; 3.70, 10; 73.50, 65; 84.00, 100; 94.00, 100. The collection was done by a fixed fraction volume of 50 mL per tube. After combining tubes based on the 254 nm and 280 nm UV traces, a total of 24 fractions were obtained. This separation yielded 31 mg of **1** (RT 74.0 min), 33.5 mg of **4** (RT 78.0 min), and 48.5 mg of **8** (RT 83.0 min). The fractions collected at RT 76.0 min (F13, 19.8 mg) and RT 81.0 min (F15, 23.0 mg) were separated in an X-Bridge C_{18} column (250×10 mm i.d., 5 μm) equipped with a Waters C_{18} precolumn cartridge holder (5×10 mm i.d., 5 μm); solvent system ACN (B) and H_2O (A), both containing 0.1% FA, in an isocratic run 50% ACN, to give **2** (1.0 mg, RT 38.5 min), and **3** (0.6 mg, RT 42.0 min); and **6** (0.5 mg, RT 45.0 min) respectively. The following separations were done using the same solvent system and column but different isocratic compositions. The fraction F17 (RT 85.0 min, 48.4 mg) was separated using an isocratic of 55% ACN to give **5** (1.0 mg, RT 36.0 min), **8** (1.7 mg, RT 38.0 min), **9** (2.2 mg, RT 41.0 min) and **10** (2.3 mg, RT 43.5 min). The fractions F18 (RT 87.5 min, 25.7 mg), and F19 (RT 88.0 min, 26.9 mg) were separated using an isocratic of 60% ACN to give **7** (0.4 mg, RT 26 min), and **11** (1.7 mg, RT 41.0 min). Finally, the fraction F20 (RT 89.0 min, 27.7 mg) was separated using an isocratic of 60% ACN to give **12** (0.4 mg, RT 41.0 min), and **13** (0.5 mg, RT 43.0 min). All the fractions were introduced in the system using a Dry-load injection (Queiroz et al., 2019).

Description of isolated compounds.

Compound **1** (Hymenotamayonin G): (2S,8R,10R,17R)-2-(5-hydroxy, 4-methoxy-3-(3-methylbut-2-en-1-yl)phenyl)-12-(2-hydroxypropan-2-yl)-8-(3-methylbut-2-en-1-yl)-5-oxotricyclo[6.3.1.0^{5,10}]dodec-5-ene-7,9-dione. Amorphous pale-yellow powder, $[\alpha]_D^{20}$ -16 (c 0.03, MeOH); UV (c 0.03, MeOH) λ_{max} 220, 269 nm.

^{1}H NMR (CD$_3$OD, 600 MHz) δ 1.21 (3H, s, H$_3$-20), 1.34 (3H, s, H$_3$-19), 1.48 (3H, d, J = 1.2 Hz, H$_3$-14), 1.50 (3H, d, J = 1.2 Hz, H$_3$-15), 1.64 (1H, overlapped, H-3eq), 1.73 (3H, d, J = 1.3 Hz, H$_3$-

4"), 1.77 (3H, d, J = 1.3 Hz, H$_3$-5"), 1.91 (1H, dd, J = 12.9, 5.5 Hz, H-16b), 2.05 (1H, dd, J = 14.3, 6.0 Hz, H-11b), 2.16 (1H, overlapped, H-4eq), 2.17 (1H, dd, J = 14.3, 7.9 Hz, H-11a), 2.28 (2H, m, H-3ax, H-4ax), 2.82 (1H, t, J = 12.9, 10.9 Hz, H-16a), 3.12 (1H, d, J = 5.4 Hz, H-2), 3.28 (2H, m, H$_2$-1"), 3.75 (3H, s, 4'-OCH$_3$), 4.72 (1H, dd, J = 10.9, 5.5 Hz, H-17), 4.76 (1H, thept, J = 7.9, 6.0, 1.2 Hz, H-12), 5.24 (1H, thept, J = 6.7, 1.3 Hz, H-2"), 5.80 (1H, s, H-6), 6.38 (1H, d, J = 2.3 Hz, H-2'), 6.47 (1H, d, J = 2.3 Hz, H-6'); ^{13}C NMR (CD$_3$OD, 151 MHz) δ 17.9 (CH$_3$-4"), 18.0 (CH$_3$-14), 25.4 (CH$_3$-20), 26.0 (CH$_3$-5"), 26.1 (CH$_3$-15), 26.5 (CH$_3$-19), 27.5 (CH$_2$-3), 29.1 (CH$_2$-1"), 30.4 (CH$_2$-11), 30.8 (CH$_2$-16), 33.1 (CH$_2$-4), 55.2 (CH-2), 60.8 (4'-OCH$_3$), 61.7 (C-10), 67.2 (C-8), 71.1 (C-18), 92.8 (CH-17), 104.3 (CH-6), 115.8 (CH-6'), 121.1 (CH-12), 121.6 (CH-2'), 123.9 (CH-2"), 133.6 (C-3"), 134.1 (C-13), 136.3 (C-3'), 137.9 (C-1'), 146.0 (C-4'), 151.0 (C-5'), 181.2 (C-5), 201.3 (C-7), 207.7 (C-9).

Supplementary Figures S.8-S13

^{1}H NMR (CDCl$_3$, 600 MHz) δ 1.25 (3H, s, H$_3$-20), 1.38 (3H, s, H$_3$-19), 1.51 (3H, s, H$_3$-14), 1.55 (3H, s, H$_3$-15), 1.67 (1H, overlapped, H-3eq), 1.73 (3H, s, H$_3$-4"), 1.77 (3H, s, H$_3$-5"), 1.85 (1H, dd, J = 13.0, 5.3 Hz, H-16b), 2.04 (1H, dd, J = 13.6, 4.9 Hz, H-4eq), 2.15 (1H, dd, J = 15.1, 5.7 Hz, H-11b), 2.25 (1H, td, J = 13.6, 4.9 Hz, H-4ax), 2.25(1H, dd, J = 15.1, 6.1 Hz, H-11a), 2.33 (1H, tt, J = 13.6, 6.1, 4.9 Hz, H-3ax), 2.83 (1H, t, J = 13.0, 11.1 Hz, H-16a), 3.24 (1H, d, J = 6.1 Hz, H-2), 3.30 (2H, d, J = 7.3 Hz, H$_2$-1"), 3.77 (3H, s, 4'OCH3), 4.57 (1H, dd, J = 11.1, 5.3 Hz, H-17), 4.77 (1H, t, J = 6.1, 5.7 Hz, H-12), 5.23 (1H, t, J = 7.3 Hz, H-2"), 5.86 (1H, s, H-6), 6.41 (1H, d, J = 2.3 Hz, H-2'), 6.53 (1H, d, J = 2.3 Hz, H-6'); ^{13}C NMR (CDCl$_3$, 151 MHz) δ 17.9 (CH$_3$-4"), 18.1 (CH$_3$-14), 24.4 (CH$_3$-20), 26.0 (CH$_3$-5", CH$_3$-15), 26.6 (CH$_2$-3), 27.0 (CH$_3$-19), 28.3 (CH$_2$-1"), 29.3 (CH$_2$-11), 30.4 (CH$_2$-16), 32.1 (CH$_2$-4), 53.8 (CH-2), 60.1 (C-10), 61.3 (4'-OCH$_3$), 66.0 (C-8), 70.9 (C-18), 91.0 (CH-17), 104.4 (CH-6), 113.1 (CH-6'), 119.7 (CH-12), 121.9 (CH-2"), 122.3 (CH-2"), 133.4 (C-3"), 133.7 (C-13), 134.5 (C-3'), 137.5 (C-1'), 144.2 (C-4'), 148.7 (C-5'), 177.7 (C-5), 198.8 (C-7) 206.4 (C-9). HRESIMS *m/z* 509.2894 [M+H]$^+$ (calculated for C$_{31}$H$_{41}$O$_6$, error -0.65 ppm,); MS/MS CCMSLIB00011431737

InChI=1S/C31H40O6/c1-18(2)8-9-20-14-21(15-23(32)27(20)36-7)22-11-12-30-17-26(29(5,6)35)37-25(30)16-24(33)31(22,28(30)34)13-10-19(3)4/h8,10,14-16,22,26,32,35H,9,11-13,17H2,1-7H3/t22-,26+,30+,31+/m0/s1

Compound **2** (Hymenotamayonin A): (2*S*,8*R*,10*R*)-2-(4,5-dihydroxy-3-(3-methylbut-2-en-1-yl)phenyl)-5-hydroxy-8,10-bis(3-methylbut-2-en-1-yl)bicyclo[3.3.1]non-6-ene-7,9-dione. Amorphous pale-yellow powder, $[\alpha]_D^{20}$ -2 (c 0.001, MeOH); UV (c 0.001, MeOH) λ$_{max}$ 213, 281 nm.

^{1}H NMR (CD$_3$OD, 600 MHz) δ 1.47 (3H, d, J = 1.5 Hz, H$_3$-14), 1.55 (3H, d, J = 1.5 Hz, H$_3$-15), 1.55 (1H, overlapped, H-3eq), 1.68 (3H, d, J = 1.5 Hz, H$_3$-20), 1.70 (3H, d, J = 1.5 Hz, H$_3$-19), 1.72 (3H, d, J = 1.4 Hz, H$_3$-4''), 1.76 (3H, d, J = 1.4 Hz, H$_3$-5''), 1.79 (1H, dd, J = 13.8, 5.2 Hz, H-4eq), 2.09 (2H, m, H$_2$-11), 2.17 (1H, td, J = 13.8, 4.9 Hz, H-4ax), 2.34 (1H, tt, J = 14.3, 5.8 Hz, H-3ax), 2.47 (1H, dd, J = 14.5, 6.9 Hz, H-16b), 2.57 (1H, dd, J = 14.5, 6.9 Hz, H-16a), 3.07 (1H, d, J = 6.4 Hz, H-2eq), 3.25 (2H, m, H$_2$-1''), 4.87 (1H, overlapped, H-12), 5.19 (1H, thept, J = 6.9, 1.5 Hz, H-17), 5.30 (1H, thept, J = 7.4, 1.4 Hz, H-2''), 6.28 (1H, d, J = 2.2 Hz, H-2'), 6.38 (1H, d, J = 2.2 Hz, H-6'); ^{13}C NMR (CD$_3$OD, 151 MHz) δ 17.9 (CH$_3$-4''), 18.0 (CH$_3$-14), 18.2 (CH$_3$-19), 26.0 (CH$_3$-5''), 26.1 (CH$_3$-15), 26.1 (CH$_3$-20), 28.1 (CH$_2$-3), 29.2 (CH$_2$-1''), 30.3 (CH$_2$-11), 31.1 (CH$_2$-16), 34.7 (CH$_2$-4), 53.8 (CH-2), 61.6 (C-10), 64.7 (C-8), 114.8 (CH-6'), 121.4 (CH-2'), 121.9 (CH-17), 122.0 (CH-12), 123.9 (CH-2''), 129.4 (C-3'), 133.2 (C-3'', C-13), 133.4 (C-1'), 133.9 (C-18), 143.0 (C-4'), 145.8 (C-5'), 211.5 (C-9). **Supplementary Figures S.14-S19**. HRESIMS m/z 479.2793 [M+H]$^+$ (calculated for C$_{30}$H$_{39}$O$_5$, error 0.21 ppm); MS/MS CCMSLIB00011431729

InChI=1S/C30H38O5/c1-18(2)7-8-21-15-22(16-24(31)27(21)34)23-11-13-29(12-9-19(3)4)25(32)17-26(33)30(23,28(29)35)14-10-20(5)6/h7,9-10,15-17,23,31-32,34H,8,11-14H2,1-6H3/t23-,29-,30+/m0/s1

Compound **3**: 3′,8-diprenylapigenin (Dat et al., 2010). Amorphous white powder, $[\alpha]_D^{20}$ -14 (c 0.0006, MeOH); UV (c 0.0006, MeOH) λ$_{max}$ 203, 276, 349 nm.

^{1}H NMR (CD$_3$OD, 600 MHz) δ 1.68 (3H, s, H$_3$-5''), 1.74 (3H, s, H$_3$-10'), 1.78 (3H, s, H$_3$-11'), 1.81 (3H, s, H$_3$-4''), 3.37 (2H, d, J = 7.4 Hz, H$_2$-7'), 3.53 (2H, d, J = 7.2 Hz, H$_2$-1''), 5.29 (1H, t, J = 7.2 Hz, H-2''), 5.36 (1H, t, J = 7.4 Hz, H-8'), 6.26 (1H, s, H-6), 6.57 (1H, s, H-3), 6.90 (1H, d, J = 8.3 Hz, H-5'), 7.69 (1H, dd, J = 8.3, 2.9 Hz, H-6'), 7.76 (1H, d, J = 2.6 Hz, H-2'); ^{13}C NMR (CD$_3$OD, 151 MHz) δ 17.9 (CH$_3$-10'), 18.2 (CH$_3$-4''), 22.6 (CH$_2$-1''), 25.9 (CH$_3$-11'), 26.0 (CH$_3$-5''), 29.0 (CH$_2$-7'), 99.6 (CH-6), 103.3 (CH-3), 105.2 (C-10), 108.2 (C-8), 116.2 (CH-5'), 123.0 (CH-8'), 123.4 (C-1'), 123.6 (CH-2''), 126.9 (CH-6'), 128.8 (CH-2'), 130.3 (C-3'), 132.7 (C-3''), 134.2 (C-9'), 156.5 (C-9), 160.5 (C-4'), 160.8 (C-5), 163.4 (C-7), 166.5 (C-2), 184.3 (C-4). **Supplementary Figures S.20-S25**. HRESIMS m/z 407.1853 [M+H]$^+$ (calculated for C$_{25}$H$_{39}$O$_5$, error 0.14 ppm); MS/MS CCMSLIB00011431727

InChI=1S/C25H26O5/c1-14(2)5-7-16-11-17(8-10-19(16)26)23-13-22(29)24-21(28)12-20(27)18(25(24)30-23)9-6-15(3)4/h5-6,8,10-13,26-28H,7,9H2,1-4H3

Compound **4** (Hymenotamayonin H): (2*S*,8*R*,10*R*,12*S*)-2-(5-hydroxy, 4-methoxy-3-(3-methylbut-2-en-1-yl)phenyl)-17-(2-hydroxypropan-2-yl)-10-(3-methylbut-2-en-1-yl-7-oxotricyclo[6.3.1.0^{7,8}]dodec-6-ene-5,9-dione. Amorphous pale-yellow powder, $[\alpha]_D^{20}$ +3 (c 0.03, MeOH); UV (c 0.03, MeOH) λ_{max} 214, 269 nm.

^{1}H NMR (CD$_3$OD, 600 MHz) δ 1.10 (3H, s, H$_3$-15), 1.28 (3H, s, H$_3$-14), 1.63 (3H, s, H$_3$-20), 1.67 (1H, overlapped, H-3eq), 1.68 (3H, s, H-$_3$19), 1.73 (3H, s, H$_3$-4"), 1.74 (1H, overlapped, H-11b), 1.76 (3H, s, H$_3$-5"), 1.78 (1H, overlapped, H-4eq), 2.08 (1H, td, *J* = 14.1, 4.8 Hz, H-4ax), 2.36 (1H, tt, *J* = 15.0, 14.1, 6.4, 5.0 Hz, H-3ax), 2.43 (1H, dd, *J* = 14.5, 6.9 Hz, H-16b), 2.53 (2H, m, H-11a, H-16a), 3.28 (2H, d, *J* = 7.4 Hz, H$_2$-1"), 3.40 (1H, d, *J* = 6.4 Hz, H-2), 3.74 (3H, s, 4'-OCH$_3$), 4.62 (1H, dd, *J* = 11.1, 5.4 Hz, H-12), 5.07 (1H, brt, *J* = 7.3 Hz, H-17), 5.23 (2H, brt, *J* = 7.4 Hz, H-2"), 5.81 (1H, s, H-6), 6.43 (1H, d, *J* = 2.3 Hz, H-2'), 6.53 (1H, d, *J* = 2.3 Hz, H-6'); ^{13}C NMR (CD$_3$OD, 151 MHz) δ 18.0 (CH$_3$-4"), 18.2 (CH$_3$-19), 25.2 (CH$_3$-15), 26.0 (CH$_3$-5"), 26.1 (CH$_3$-20), 26.3 (CH$_3$-14), 27.8 (CH$_2$-3), 28.7 (CH$_2$-11), 29.2 (CH$_2$-1"), 31.1 (CH$_2$-16), 34.9 (CH$_2$-4), 49.4 (CH-2), 60.8 (4'-OCH$_3$), 64.4 (C-10), 64.7 (C-8), 71.1 (C-13), 92.2 (CH-12), 104.7 (CH-6), 115.9 (CH-6'), 121.1 (CH-17), 121.3 (CH-2'), 123.8 (CH-2"), 133.6 (C-3"), 134.5 (C-18), 136.7 (C-3'), 138.1 (C-1'), 146.1 (C-4'), 151.4 (C-5'), 182.1 (C-7), 200.7 (C-5), 208.0 (C-9). **Supplementary Figures S.26-S31**. HRESIMS *m/z* 509.2894 [M+H]$^+$ (calculated for C$_{31}$H$_{41}$O$_6$, error -0.65 ppm); MS/MS CCMSLIB00011431736

InChI=1S/C31H40O6/c1-18(2)8-9-20-14-21(15-23(32)27(20)36-7)22-11-13-30(12-10-19(3)4)24(33)16-25-31(22,28(30)34)17-26(37-25)29(5,6)35/h8,10,14-16,22,26,32,35H,9,11-13,17H2,1-7H3/t22-,26-,30-,31+/m0/s1

Compound **5**: 6,8-diprenylapigenin (Lin et al., 2017b). Amorphous white powder, $[\alpha]_D^{20}$ -15 (c 0.001, MeOH); UV (c 0.001, MeOH) λ_{max} 207, 281, 337 nm.

^{1}H NMR (CD$_3$OD, 600 MHz) δ 1.68 (3H, d, *J* = 1.4 Hz, H$_3$-5"), 1.70 (3H, d, *J* = 1.5 Hz, H$_3$-5'''), 1.80 (3H, d, *J* = 1.4 Hz, H$_3$-4"), 1.84 (3H, d, *J* = 1.5 Hz, H$_3$-4'''), 3.39 (2H, d, *J* = 7.2 Hz, H$_2$-1"), 3.60 (2H, d, *J* = 6.6 Hz, H$_2$-1'''), 5.21 (2H, m, H-2", H-2'''), 6.60 (1H, s, H-3), 6.93 (2H, d, *J* = 8.8 Hz, H-3', H-5'), 7.85 (2H, d, *J* = 8.8 Hz, H-2', H-6'); ^{13}C NMR (CD$_3$OD, 151 MHz) δ 18.0 (CH$_3$-4"), 18.3 (CH$_3$-4'''), 22.5 (CH$_2$-1"), 23.0 (CH$_2$-1'''), 25.9 (CH$_3$-5'''), 26.0 (CH$_3$-5"), 103.6 (CH-3), 105.5 (C-10), 108.2 (C-8), 113.3 (C-6), 117.0 (CH-3', CH-5'), 123.2 (CH-2"), 123.7 (C-1'), 123.9 (CH-2'''), 129.5 (CH-2', CH-6'), 132.8 (C-3"), 133.0 (C-3'''), 154.6 (C-9), 157.9 (C-5), 160.8 (C-7), 162.7 (C-4'), 166.1

(C-2), 184.4 (C-4). **Supplementary Figures S.32-S37**. HRESIMS m/z 407.1853 [M+H]$^+$ (calculated for $C_{25}H_{27}O_5$, error 0.14 ppm); MS/MS

InChI=1S/C25H26O5/c1-14(2)5-11-18-23(28)19(12-6-15(3)4)25-22(24(18)29)20(27)13-21(30-25)16-7-9-17(26)10-8-16/h5-10,13,26,28-29H,11-12H2,1-4H3

Compound **6** (Hymenotamayonin I): (2*S*,8*R*,10*R*,17*R*)-17-hydroxy-2-(5-hydroxy, 4-methoxy-3-(3-methylbut-2-en-1-yl)phenyl)-18,18-dimethyl-8-(3-methylbut-2-en-1-yl)-5-oxotricyclo[7.3.1.0^{5,10}]dodec-5-ene-7,9-dione. Amorphous pale-yellow powder, $[\alpha]_D^{20}$ +18 (c 0.0005, MeOH); UV (c 0.0005, MeOH) λ_{max} 207, 273 nm.

^{1}H NMR (CD$_3$OD, 600 MHz) δ 1.26 (3H, s, H$_3$-20), 1.44 (3H, s, H$_3$-19), 1.47 (3H, d, J = 1.4 Hz, H$_3$-14), 1.53 (3H, d, J = 1.4 Hz, H$_3$-15), 1.55 (1H, brd, J = 10.8 Hz, H-3eq), 1.74 (1H, dd, J = 14.9, 5.3 Hz, H-16b), 1.74 (3H, d, J = 1.3 Hz, H$_3$-4"), 1.79 (3H, d, J = 1.3 Hz, H$_3$-5"), 2.09 (1H, td, J = 14.5, 4.6 Hz, H-4ax), 2.07 (1H, overlapped, H-11b), 2.15 (1H, dd, J = 14.7, 7.8 Hz, H-11a), 2.26 (1H, tt, J = 14.2, 5.6 Hz, H-3ax), 2.63 (1H, dd, J = 14.5, 4.9 Hz, H-4eq), 2.94 (1H, dd, J = 14.9, 3.9 Hz, H-16a), 3.03 (1H, d, J = 6.2 Hz, H-2eq), 3.28 (2H, d, J = 7.5 Hz, H$_2$-1"), 3.75 (3H, s, 4'-OCH$_3$), 3.79 (1H, t, J = 5.3, 3.9 Hz, H-17), 4.81 (1H, thept, J = 7.8, 1.4 Hz, H-12), 5.25 (1H, thept, J = 7.5, 1.3 Hz, H-2"), 5.88 (1H, s, H-6), 6.31 (1H, d, J = 2.3 Hz, H-2'), 6.42 (1H, d, J = 2.3 Hz, H-6'); ^{13}C NMR (CD$_3$OD, 151 MHz) δ 17.9 (CH$_3$-4"), 18.0 (CH$_3$-14), 24.0 (CH$_3$-19), 26.1 (CH$_3$-5"), 26.1 (CH$_3$-15), 26.9 (CH$_3$-20), 27.3 (CH$_2$-3), 29.0 (CH$_2$-1"), 30.5 (CH$_2$-11), 31.5 (CH$_2$-16), 36.2 (CH$_2$-4), 51.6 (C-10), 55.0 (CH-2), 60.8 (4'-OCH$_3$), 67.5 (C-8), 69.9 (CH-17), 84.8 (C-18), 114.7 (CH-6), 116.1 (CH-6'), 121.2 (CH-12), 121.4 (CH-2'), 123.8 (CH-2"), 133.8 (C-3"), 134.0 (C-13), 136.2 (C-3'), 138.1 (C-1'), 145.9 (C-4'), 151.0 (C-5'), 176.5 (C-5), 200.7 (C-7), 209.7 (C-9). Supplementary **Supplementary Figures S.38-S43**. HRESIMS m/z 509.2894 [M+H]$^+$ (calculated for $C_{31}H_{41}O_6$, error -0.65 ppm); MS/MS

InChI=1S/C31H40O6/c1-18(2)8-9-20-14-21(15-23(32)27(20)36-7)22-11-12-30-17-25(34)29(5,6)37-26(30)16-24(33)31(22,28(30)35)13-10-19(3)4/h8,10,14-16,22,25,32,34H,9,11-13,17H2,1-7H3/t22-,25+,30+,31+/m0/s1

Compound **7**: 3′,6-diprenyl-diprenylapigenin (Fukai et al., 1991). Amorphous white powder, $[\alpha]_D^{20}$ -23 (c 0.0004, MeOH); UV (c 0.0004, MeOH) λ_{max} 206, 275, 343 nm.

^{1}H NMR (CD$_3$OD, 600 MHz) δ 1.67 (3H, d, J = 1.4 Hz, H$_3$-5''), 1.76 (3H, d, J = 1.3 Hz, H$_3$-10'), 1.79 (6H, d, J = 1.4 Hz, H$_3$-4'', H$_3$-11'), 3.32 (2H, overlapped, H$_2$-1''), 3.36 (2H, d, J = 7.4 Hz, H$_2$-7'), 5.24 (1H, thept, J = 7.0, 1.4 Hz, H-2''), 5.36 (1H, thept, J = 7.4, 1.3 Hz, H-8'), 6.48 (1H, s, H-8), 6.55 (1H, s, H-3), 6.89 (1H, d, J = 9.0 Hz, H-3'), 7.67 (2H, m, H-2', H-6'); ^{13}C NMR (CD$_3$OD, 151 MHz) δ 17.9 (CH$_3$-4'', CH$_3$-10'), 22.3 (CH$_2$-1''), 25.8 (CH$_3$-11'), 26.0 (CH$_3$-5''), 29.2 (CH$_2$-7'), 94.1 (CH-8), 103.6 (CH-3), 105.1 (C-10), 113.1 (C-6), 116.2 (CH-3'), 123.2 (CH-8', C-1'), 123.4 (CH-2''), 126.8 (CH-2'), 128.9 (CH-6'), 130.4 (C-5'), 132.2 (C-3''), 134.0 (C-9'), 157.4 (C-9), 159.9 (C-5), 160.5 (C-4'), 163.7 (C-7), 166.4 (C-2), 184.1 (C-4). **Supplementary Figures S.44-S48**; . HRESIMS m/z 407.1853 [M+H]$^+$ (calculated for C$_{25}$H$_{27}$O$_5$, error 0.22 ppm); MS/MS CCMSLIB00011431728

InChI=1S/C25H26O5/c1-14(2)5-7-16-11-17(8-10-19(16)26)22-13-21(28)24-23(30-22)12-20(27)18(25(24)29)9-6-15(3)4/h5-6,8,10-13,26-27,29H,7,9H2,1-4H3

Compound **8** (Hymenotamayonin C): (2S,8R,10R)-2-(5-hydroxy-4-methoxy-3-(3-methylbut-2-en-1-yl)phenyl)-5-hydroxy-8,10-bis(3-methylbut-2-en-1-yl)bicyclo[3.3.1]non-6-ene-7,9-dione. Amorphous orange powder, $[\alpha]_D^{20}$ -14 (c 0.001, MeOH); UV (c 0.001, MeOH) λ$_{max}$ 219, 271 nm.

^{1}H NMR (CD$_3$OD, 600 MHz) δ 1.46 (3H, d, J = 1.5 Hz, H$_3$-14), 1.55 (3H, d, J = 1.5 Hz, H$_3$-15), 1.56 (1H, overlapped, H-3eq), 1.68 (3H, d, J = 1.4 Hz, H$_3$-19), 1.70 (3H, d, J = 1.4 Hz, H$_3$-20), 1.74 (3H, d, J = 1.4 Hz, H$_3$-4''), 1.76 (3H, d, J = 1.4 Hz, H$_3$-5''), 1.79 (1H, overlapped, H-4eq), 2.08 (1H, dd, J = 14.2, 5.2 Hz, H-11b), 2.15 (1H, overlapped, H-11a), 2.17 (1H, td, J = 13.8, 4.7 Hz, H-4ax), 2.31 (1H, tt, J = 13.8, 6.4 Hz, H-3ax), 2.49 (1H, dd, J = 14.5, 7.1 Hz, H-16b), 2.58 (1H, dd, J = 14.5, 7.1 Hz, H-16a), 3.12 (1H, d, J = 6.4 Hz, H-2eq), 3.27 (2H, m, H$_2$-1''), 3.74 (3H, s, 4'-OCH$_3$), 4.87 (1H, overlapped, H-12), 5.19 (1H, thept, J = 7.1, 1.5 Hz, H-17), 5.25 (1H, thept, J = 7.5, 1.4 Hz, 2''), 6.34 (1H, d, J = 2.3 Hz, H-2'), 6.44 (1H, d, J = 2.3 Hz, H-6'); ^{13}C NMR (CD$_3$OD, 151 MHz) δ 18.0 (CH$_3$-4'', CH$_3$-14), 18.2 (CH$_3$-19), 26.0 (CH$_3$-5''), 26.1 (CH$_3$-15), 26.2 (CH$_3$-20), 27.8 (CH$_2$-3), 29.3 (CH$_2$-1''), 30.1 (CH$_2$-11), 30.9 (CH$_2$-16), 34.5 (CH$_2$-4), 53.6 (CH-2), 60.8 (4'-OCH$_3$), 116.2 (CH-6'), 121.4 (CH-12, CH-17), 121.6 (CH-2'), 124.0 (CH-2''), 133.4 (C-3''), 133.8 (C-13), 134.4 (C-18), 136.2 (C-3'), 138.2 (C-1'), 145.9 (C-4'), 150.9 (C-5'), 210.4 (C-9). **Supplementary Figures S49-S54**. HRESIMS m/z 493.2894 [M+H]$^+$ (calculated for C$_{31}$H$_{41}$O$_5$, error -0.34 ppm); MS/MS CCMSLIB00011431733

InChI=1S/C31H40O5/c1-19(2)8-9-22-16-23(17-25(32)28(22)36-7)24-12-14-30(13-10-20(3)4)26(33)18-27(34)31(24,29(30)35)15-11-21(5)6/h8,10-11,16-18,24,32-33H,9,12-15H2,1-7H3/t24-,30-,31+/m0/s1

Compound **9** (Hymenotamayonin J): (2*S*,8*R*,10*R*,12*S*)-12-hydroxy-2-(5-hydroxy, 4-methoxy-3-(3-methylbut-2-en-1-yl)phenyl)-13,13-dimethyl-10-(3-methylbut-2-en-1-yl)-7-oxotricyclo[7.3.1.0^{7,8}]dodec-5-ene-5,9-dione. Amorphous orange powder, $[\alpha]_D^{20}$ -20 (c 0.002, MeOH); UV (c 0.002, MeOH) λ_{max} 217, 276, 344 nm.

^{1}H NMR (CD$_3$OD, 600 MHz) δ 1.46 (3H, d, *J* = 1.5 Hz, H$_3$-14), 1.55 (3H, d, *J* = 1.5 Hz, H$_3$-15), 1.56 (1H, overlapped, H-3eq), 1.68 (3H, d, *J* = 1.4 Hz, H$_3$-19), 1.70 (3H, d, *J* = 1.4 Hz, H$_3$-20), 1.74 (3H, d, *J* = 1.4 Hz, H$_3$-4"), 1.76 (3H, d, *J* = 1.4 Hz, H$_3$-5"), 1.79 (1H, overlapped, H-4eq), 2.08 (1H, dd, *J* = 14.2, 5.2 Hz, H-11b), 2.15 (1H, overlapped, H-11a), 2.17 (1H, td, *J* = 13.8, 4.7 Hz, H-4ax), 2.31 (1H, tt, *J* = 13.8, 6.4 Hz, H-3ax), 2.49 (1H, dd, *J* = 14.5, 7.1 Hz, H-16b), 2.58 (1H, dd, *J* = 14.5, 7.1 Hz, H-16a), 3.12 (1H, d, *J* = 6.4 Hz, H-2eq), 3.27 (2H, m, H$_2$-1"), 3.74 (3H, s, 4'-OCH$_3$), 4.87 (1H, overlapped, H-12), 5.19 (1H, thept, *J* = 7.1, 1.5 Hz, H-17), 5.25 (1H, thept, *J* = 7.5, 1.4 Hz, 2"), 6.34 (1H, d, *J* = 2.3 Hz, H-2'), 6.44 (1H, d, *J* = 2.3 Hz, H-6'); ^{13}C NMR (CD$_3$OD, 151 MHz) δ 18.0 (CH$_3$-4", CH$_3$-14), 18.2 (CH$_3$-19), 26.0 (CH$_3$-5"), 26.1 (CH$_3$-15), 26.2 (CH$_3$-20), 27.8 (CH$_2$-3), 29.3 (CH$_2$-1"), 30.1 (CH$_2$-11), 30.9 (CH$_2$-16), 34.5 (CH$_2$-4), 53.6 (CH-2), 60.8 (4'-OCH$_3$), 116.2 (CH-6'), 121.4 (CH-12, CH-17), 121.6 (CH-2'), 124.0 (CH-2"), 133.4 (C-3"), 133.8 (C-13), 134.4 (C-18), 136.2 (C-3'), 138.2 (C-1'), 145.9 (C-4'), 150.9 (C-5'), 210.4 (C-9). **Supplementary Figures S.55-S60**. HRESIMS *m/z* 509.2893 [M+H]$^+$ (calculated for C$_{31}$H$_{41}$O$_6$, error -0.83 ppm); MS/MS CCMSLIB00011431738

InChI=1S/C31H40O6/c1-18(2)8-9-20-14-21(15-23(32)27(20)36-7)22-11-13-30(12-10-19(3)4)24(33)16-26-31(22,28(30)35)17-25(34)29(5,6)37-26/h8,10,14-16,22,25,32,34H,9,11-13,17H2,1-7H3/t22-,25-,30-,31+/m0/s1

Compound **10** (Hymenotamayonin B): (2*R*,8*R*,10*R*)-2-(4,5-dihydroxy-3-(3-methylbut-2-en-1-yl)phenyl)-5-hydroxy-8,10-bis(3-methylbut-2-en-1-yl)bicyclo[3.3.1]non-6-ene-7,9-dione. Amorphous orange powder, $[\alpha]_D^{20}$ -12 (c 0.002, MeOH); UV (c 0.002, MeOH) λ_{max} 221, 273 nm.

^{1}H NMR (CD$_3$OD, 600 MHz) δ 1.51 (3H, d, *J* = 1.5 Hz, H$_3$-14), 1.59 (3H, d, *J* = 1.5 Hz, H$_3$-15), 1.63 (3H, d, *J* = 1.5 Hz, H$_3$-20), 1.64 (1H, overlapped, H-4ax), 1.69 (3H, d, *J* = 1.5 Hz, H$_3$-19), 1.71 (3H, d, *J* = 1.4 Hz, H$_3$-4"), 1.71 (1H, overlapped, H-3eq), 1.73 (3H, d, *J* = 1.4 Hz, H$_3$-5"), 1.97

(1H, ddd, J = 13.1, 4.9, 1.8 Hz, H-4eq), 2.21 (2H, m, H-3ax, H-11b), 2.30 (1H, dd, J = 15.0, 6.7 Hz, H-11a), 2.48 (2H, m, H$_2$-16), 2.64 (1H, dd, J = 13.2, 4.0 Hz, H-2ax), 3.23 (1H, dd, J = 15.6, 7.4 Hz, H-1"b), 3.28 (1H, dd, J = 15.6, 7.4 Hz, H-1"a), 4.87 (1H, overlapped, H-12), 4.97 (1H, thept, J = 6.9, 1.5 Hz, H-17), 5.29 (1H, thept, J = 7.4, 1.4 Hz, H-2"), 6.32 (1H, d, J = 2.2 Hz, H-2'), 6.40 (1H, d, J = 2.2 Hz, H-6'); ^{13}C NMR (CD$_3$OD, 151 MHz) δ 17.9 (CH$_3$-4"), 18.2 (CH$_3$-14, CH$_3$-19), 26.0 (CH$_3$-5"), 26.1 (CH$_3$-15), 26.1 (CH$_3$-20), 28.1 (CH$_2$-3), 29.2 (CH$_2$-1"), 29.8 (CH$_2$-11), 30.9 (CH$_2$-16), 39.2 (CH$_2$-4), 56.2 (CH-2), 114.4 (CH-6'), 121.4 (CH-17), 121.9 (CH-12), 122.6 (CH-2'), 124.2 (CH-2"), 128.7 (C-3'), 131.3 (C-1'), 132.7 (C-3"), 133.3 (C-13), 134.0 (C-18), 143.4 (C-4'), 145.3 (C-5'), 211.0 (C-9). **Supplementary Figures S.61-S66**. HRESIMS m/z 479.2791 [M+H]$^+$ (calculated for C$_{30}$H$_{39}$O$_5$, error -0.19 ppm); MS/MS CCMSLIB00011431730

InChI=1S/C30H38O5/c1-18(2)7-8-21-15-22(16-24(31)27(21)34)23-11-13-29(12-9-19(3)4)25(32)17-26(33)30(23,28(29)35)14-10-20(5)6/h7,9-10,15-17,23,31-32,34H,8,11-14H2,1-6H3/t23-,29+,30-/m1/s1

Compound **11** (Hymenotamayonin D): (2*R*,8*R*,10*R*)-2-(5-hydroxy-4-methoxy-3-(3-methylbut-2-en-1-yl)phenyl)-5-hydroxy-8,10-bis(3-methylbut-2-en-1-yl)bicyclo[3.3.1]non-6-ene-7,9-dione. Amorphous pale-yellow powder, $[\alpha]_D^{20}$ -27 (c 0.0008, MeOH); UV (c 0.0008, MeOH) λ$_{max}$ 207, 286 nm.

^{1}H NMR (CD$_3$OD, 600 MHz) δ 1.51 (3H, d, J = 1.6 Hz, H$_3$-14), 1.60 (3H, d, J = 1.6 Hz, H$_3$-15), 1.63 (3H, d, J = 1.3 Hz, H$_3$-20), 1.63 (1H, overlapped, H-4ax), 1.69 (3H, d, J = 1.3 Hz, H$_3$-19), 1.71 (1H, overlapped, H-3eq), 1.73 (6H, d, J = 1.3 Hz, H$_3$-4", H$_3$-5"), 1.98 (1H, ddd, J = 12.9, 4.8, 1.8 Hz, H-4eq), 2.18 (1H, dd, J = 14.9, 7.2 Hz, H-11b), 2.25 (1H, td, J = 13.1, 4.8 Hz, H-3ax), 2.32 (1H, dd, J = 14.9, 7.2 Hz, H-11a), 2.46 (1H, dd, J = 14.3, 7.0 Hz, H-16b), 2.50 (1H, dd, J = 14.3, 7.0 Hz, 16a), 2.68 (1H, dd, J = 13.1, 4.0 Hz, H-2ax), 3.27 (2H, m, H$_2$-1"), 3.73 (3H, s, 4'-OCH$_3$), 4.89 (1H, overlapped, H-12), 4.98 (1H, thept, J = 7.0, 1.6 Hz, H-17), 5.24 (1H, thept, J = 7.2, 1.3 Hz, H-2"), 6.38 (1H, d, J = 2.2 Hz, H-2'), 6.47 (1H, d, J = 2.2 Hz, H-6'); ^{13}C NMR (MeOD, 151 MHz) δ 18.0 (CH$_3$-4"), 18.2 (CH$_3$-14, CH$_3$-19), 25.9 (CH$_3$-5"), 26.1 (CH$_3$-15), 26.1 (CH$_3$-20), 28.2 (CH$_2$-3), 29.4 (CH$_2$-1"), 29.7 (CH$_2$-11), 31.0 (CH$_2$-16), 39.0 (CH$_2$-4), 55.7 (CH-2), 60.7 (4'-OCH$_3$), 116.0 (CH-6'), 121.6 (CH-17), 122.0 (CH-12), 122.9 (CH-2'), 124.5 (CH-2"), 132.9 (C-3"), 133.1 (C-13), 134.1 (C-18), 135.4 (C-3'), 136.6 (C-1'), 146.2 (C-4'), 150.4 (C-5'), 211.1 (C-9). **Supplementary Figures S.67-S72**. HRESIMS m/z 493.2947 [M+H]$^+$ (calculated for C$_{31}$H$_{41}$O$_5$, error -0.28 ppm); MS/MS CCMSLIB00011431732

InChI=1S/C31H40O5/c1-19(2)8-9-22-16-23(17-25(32)28(22)36-7)24-12-14-30(13-10-20(3)4)26(33)18-27(34)31(24,29(30)35)15-11-21(5)6/h8,10-11,16-18,24,32-33H,9,12-15H2,1-7H3/t24-,30+,31-/m1/s1

Compound **12** (Hymenotamayonin F): (2*S*,8*R*,10*R*)-2-(5-hydroxy, 4-methoxy-3-(3-methylbut-2-en-1-yl)phenyl)-18,18-dimethyl-8-(3-methylbut-2-en-1-yl)-5-oxotricyclo[7.3.1.0^{5,10}]dodec-5-ene-7,9-dione. Amorphous pale-yellow powder, $[\alpha]_D^{20}$ +6 (c 0.0004, MeOH); UV (c 0.0004, MeOH) λ_{max} 205, 273 nm.

^{1}H NMR (CD$_3$OD, 600 MHz) δ 1.29 (3H, s, H$_3$-20), 1.46 (3H, s, H$_3$-19), 1.47 (3H, d, *J* = 1.3 Hz, H$_3$-14), 1.54 (3H, d, *J* = 1.3 Hz, H$_3$-15), 1.63 (1H, m, H-3eq), 1.71 (1H, dt, *J* = 14.4, 4.2 Hz, H-16eq), 1.73 (3H, d, *J* = 1.3 Hz, H$_3$-4''), 1.78 (3H, d, *J* = 1.3 Hz, H$_3$-5''), 1.86 (1H, dt, *J* = 14.3, 4.1 Hz, H-17eq), 1.96 (1H, td, *J* = 13.3, 4.5 Hz, H-4ax), 2.04 (1H, td, *J* = 14.3, 4.1 Hz, H-17ax), 2.06 (1H, dd, *J* = 14.7, 6.1 Hz, H-11b), 2.16 (1H, dd, *J* = 14.7, 7.8 Hz, H-11a), 2.23 (1H, m, H-3ax), 2.28 (1H, dd, *J* = 13.3, 4.5 Hz, H-4eq), 2.56 (1H, td, *J* = 14.4, 4.2 Hz, H-16ax), 3.04 (1H, d, *J* = 6.2 Hz, H-2eq), 3.28 (2H, m, H$_2$-1''), 3.74 (3H, s, 4'-OCH$_3$), 4.83 (1H, thept, *J* = 7.6, 1.3 Hz, H-12), 5.24 (1H, thept, *J* = 7.5, 1.3 Hz, H-2''), 5.82 (1H, s, H-6), 6.31 (1H, d, *J* = 2.3 Hz, H-2'), 6.41 (1H, d, *J* = 2.3 Hz, H-6'); ^{13}C NMR (CD$_3$OD, 151 MHz) δ 17.9 (CH$_3$-14), 18.0 (CH$_3$-4''), 24.2 (CH$_2$-16), 26.0 (CH$_3$-15), 26.1 (CH$_3$-5''), 26.2 (CH$_3$-20), 27.6 (CH$_2$-3), 29.0 (CH$_2$-1''), 30.1 (CH$_3$-19), 30.3 (CH$_2$-11), 31.2 (CH$_2$-17), 33.2 (CH$_2$-4), 51.0 (C-10), 54.7 (CH-2), 60.8 (4'-OCH$_3$), 67.8 (C-8), 82.3 (C-18), 113.8 (CH-6), 115.9 (CH-6'), 121.3 (CH-12), 121.4 (CH-2'), 123.8 (CH-2''), 134.0 (C-3''), 136.3 (C-3'), 138.1 (C-1'), 145.9 (C-4'), 151.0 (C-5'), 176.8 (C-5), 200.4 (C-7), 210.3 (C-9).**Supplementary Figures S.73-S78**. HRESIMS *m/z* 491.2747 [M+H]$^+$ (calculated for C$_{31}$H$_{41}$O$_5$, error -0.16 ppm); MS/MS CCMSLIB00011431734

InChI=1S/C31H40O5/c1-19(2)8-9-21-16-22(17-24(32)27(21)35-7)23-11-12-30-15-14-29(5,6)36-26(30)18-25(33)31(23,28(30)34)13-10-20(3)4/h8,10,16-18,23,32H,9,11-15H2,1-7H3/t23-,30+,31+/m0/s1

Compound **13** (Hymenotamayonin E): (2*S*,8*R*,10*R*,17*R*)-2-(5-hydroxy, 4-methoxy-3-(3-methylbut-2-en-1-yl)phenyl)-8-(3-methylbut-2-en-1-yl)-17-(prop-1-en-2-yl-5-oxotricyclo[6.3.1.0^{5,10}]dodec-5-ene-7,9-dione. Amorphous pale-yellow powder, $[\alpha]_D^{20}$ +0.4 (c 0.0005, MeOH); UV (c 0.0005, MeOH) λ_{max} 204, 270 nm.

^{1}H NMR (CD$_3$OD, 600 MHz) δ 1.49 (3H, d, *J* = 1.4 Hz, H$_3$-14), 1.53 (3H, d, *J* = 1.4 Hz, H$_3$-15), 1.66 (1H, m, H-3eq), 1.73 (3H, d, *J* = 1.3 Hz, H$_3$-4''), 1.77 (3H, d, *J* = 1.3 Hz, H$_3$-5''), 1.78 (3H, t,

J = 1.2 Hz, H$_3$-19), 2.07 (1H, dd, J = 14.5, 6.0 Hz, H-11b), 2.12 (1H, dd, J = 13.0, 5.4 Hz, H-16b), 2.17 (1H, dd, J = 14.5, 7.7 Hz, H-11a), 2.23 (1H, brd, J = 9.4 Hz, H-4eq), 2.30 (1H, overlapped, H-4ax), 2.32 (1H, overlapped, H-3ax), 2.63 (1H, dd, J = 13.0, 11.2 Hz, 16a), 3.14 (1H, d, J = 3.8 Hz, H-2eq), 3.75 (3H, s, 4'-OCH$_3$), 4.78 (1H, ddhept, J = 7.7, 6.0, 1.4 Hz, H-12), 5.05 (1H, p, J = 1.2 Hz, 20b), 5.17 (1H, q, J = 1.2 Hz, 20a), 5.25 (2H, thept, J = 7.5, 1.3 Hz, 2"), 5.32 (1H, dd, J = 11.2, 5.4 Hz, H-17), 5.80 (1H, s, H-6), 6.38 (1H, d, J = 2.3 Hz, H-2'), 6.47 (1H, d, J = 2.3 Hz, H-6'); ^{13}C NMR (CD$_3$OD, 151 MHz) δ 17.3 (CH$_3$-19), 17.9 (CH$_3$-14), 18.0 (CH$_3$-4"), 26.0 (CH$_3$-15), 26.1 (CH$_3$-5"), 27.6 (CH$_2$-3), 29.1 (CH$_2$-1"), 30.5 (CH$_2$-11), 32.6 (CH$_2$-4), 35.4 (CH$_2$-16), 55.3 (CH-2), 60.8 (4'-OCH$_3$), 61.7 (C-10), 67.3 (C-8), 89.2 (CH-17), 104.2 (CH-6), 114.4 (CH$_2$-20), 115.8 (CH-6'), 121.0 (CH-12), 121.6 (CH-2'), 123.9 (CH-2"), 133.5 (C-3"), 134.2 (C-13), 136.4 (C-3'), 137.9 (C-1'), 143.1 (C-18), 146.0 (C-4'), 151.1 (C-5'), 180.9 (C-5), 201.3 (C-7), 207.8 (C-9). **Supplementary Figures S.79-S84**. HRESIMS m/z 491.2792 [M+H]$^+$ (calculated for C$_{31}$H$_{39}$O$_5$, error 0.08 ppm); MS/MS CCMSLIB00011431731

InChI=1S/C31H38O5/c1-18(2)8-9-21-14-22(15-24(32)28(21)35-7)23-11-12-30-17-25(20(5)6)36-27(30)16-26(33)31(23,29(30)34)13-10-19(3)4/h8,10,14-16,23,25,32H,5,9,11-13,17H2,1-4,6-7H3/t23-,25+,30+,31+/m0/s1

Electronic Circular Dichroism calculations (ECD).

The absolute configuration assigned for all compounds was based on a comparison between the calculated and experimental ECD. The calculations were based on the relative configuration determined through NMR 2D ROESY experiments. The structures were used to find the conformers through a random rotor search algorithm (number of conformers, 100) employing the MMFF94s force field in Avogrado v1.2.0 (Hanwell et al., 2012). The conformers were further optimized using PM3 and B3LYP/6-31G(d,p) basis sets in Gaussian 16 software (© 2015-2022, Gaussian Inc., Wallingford, CT, USA) with the SCRF model in methanol (Nugroho and Morita, 2014; Mándi and Kurtán, 2019). All optimized conformers were checked for imaginary frequencies. The conformers were subjected to ECD calculations using TD-DFT B3LYP/def2svp as a basis set and an SCRF model in methanol in Gaussian16 software. The calculated ECD spectrum was generated in SpecVis1.71 software (Berlin, Germany) based on a Boltzmann-weighted average. Supplementary **Figure S6** shows the results. The ECD calculations were performed on the HPC Baoab cluster at the University of Geneva.

UHPLC-HRMS[2] Analysis.

Analyses were performed with a Vanquish Horizon (Thermo Scientific, Germany) equiped with a binary pump H, a dual split sampler HT and a Diode Array detector FG coupled to an Orbitrap Exploris 120 mass spectrometer (Thermo Scientific, Germany) and a Corona Veo RS Charged Aerosol Detector (CAD, Thermo Scientific, Germany). The Orbitrap employs a heated electrospray ionization source (H-ESI) with the following parameters: spray voltage: +3.5 kV; ion transfer tube temperature: 320.00 °C; vaporizer temperature: 320.00 °C; S-lens RF: 45 (arb units); sheath gas flow rate: 35.00 (arb units); Sweep Gas (arb): 1, and auxiliary gas flow rate: 10.00 (arb. units).

The mass analyzer was calibrated using a mixture of caffeine, methionine−arginine−phenylalanine− alanine−acetate (MRFA), sodium dodecyl sulfate, sodium taurocholate, and Ultramark 1621 in an acetonitrile/methanol/water solution containing 1% formic acid by direct injection. Control of the instruments was done using Thermo Scientific Xcalibur software v. 4.6.67.17. Full scans were acquired at a resolution of 30,000 fwhm (at m/z 200) and MS2 scans at 15000 fwhm in the range of 100−1000 m/z, with 1 microscan, time (ms): 200 ms, an RF lens (%): 70; AGC target custom (Normalized AGC target (%): 300); maximum injection time (ms): 130; Microscans: 1; data type: profile; Use EASY-IC(TM): ON. The Dynamic exclusion mode: Custom; Exclude after n times: 1; Exclusion duration (s): 5; Mass tolerance: ppm; low: 10, high: 10, Exclude isotopes: true. Apex detention: Desired Apex Window (%): 50. Isotope Exclusion: Assigned and unassigned with an exclusion window (m/z) for unassigned isotopes: 8. The Intensity threshold was set to 2.5E5. and a targeted mass exclusion list was used. The centroid data-dependent MS[2] (dd-MS[2]) scan acquisition events were performed in discovery mode, triggered by Apex detection with a trigger detection (%) of 300 with a maximum injection time of 120 ms, performing 1 microscan. The top 3 abundant precursors (charge states 1 and 2) within an isolation window of 1.2 m/ z were considered for MS/MS analysis. For precursor fragmentation in the HCD mode, a normalized collision energy of 15, 30, 45 % was used. Data was recorded in profile mode (Use EASY-IC(TM): ON).

The chromatographic separation was done on a Waters BEH C18 column (50 × 2.1 mm i.d., 1.7 μm, Waters, Milford, MA) using a gradient as follows (time (min), %B):0.5,8.2; 7,99; 8,99; 8.10,8.2; 9.75, 8.2. The mobile phases were (A) water with 0.1% formic acid and (B) acetonitrile with 0.1% formic acid. The flow rate was set to 600 µL/min, the injection volume was 1 μL, and the column was kept at 40 °C. The PDA detector was used from 210 to 400 nm with a resolution of 1.2 nm. The CAD was kept at 40 °C, 5 bar N$_2$, and power function 1 for a data collection rate of 20 Hz.

Data Conversion. All raw data files were converted using ThermoRawFileParser v.1.4.0.101 (https://github.com/compomics/ThermoRawFileParser)(Hulstaert et al., 2020).

MZmine Data Preprocessing.

The converted files were processed with MZmine3 (Schmid et al., 2023). For mass detection at the MS^1 level, the noise level was set to $1.0E^6$. For MS^2 detection, the noise level was set to 0.00. The ADAP chromatogram builder parameters were set as follows: Minimum consecutive scans, 5; Minimum intensity for consecutive scans, $1.0E^6$; Minimum absolute height, $1.0E^6$, and *m/z* tolerance of 0.0020 or 10.0 ppm. The Local minimum feature resolver algorithm was used for chromatogram deconvolution with the following parameters: Chromatographic threshold, 80; Minimum search range RT/Mobility (absolute), 0.10; Minimum relative height, 1 %; Minimum absolute height, $1.0E^6$; Min ratio of peak top/edge, 1.0; peak duration range, 0.01 - 1.0 min; Minimum scans, 5. Isotopes were detected using the ^{13}C isotope filter with an *m/z* tolerance of 0.0050 or 8.0 ppm, a Retention Time tolerance of 0.05 min (absolute), the maximum charge set at 2, and the representative isotope used was the most intense. Each file was filtered to remove duplicates using the Duplicate peak filter with an *m/z* tolerance of 0.005 or 10 ppm and an RT tolerance of 0.10 min. The Feature list row filter was used to filter with the following parameters: Minimum features in an isotope pattern, 2; Retention time, 0.50 - 7.00 min; Feature duration range: 0.1-1.0 min; and only the ions with an associated MS^2 spectrum were kept. The resulting filtered list was subjected to Ion Identity Networking (Schmid et al., 2021) starting with the metaCorrelate module (RT tolerance, 0.10 min; minimum height, $1.0E^5$; Intensity correlation threshold $1.0E^5$ and the Correlation Grouping with the default parameters). Followed by the Ion identity networking (*m/z* tolerance, 8.0 ppm; check: one feature; Minimum height: $1.0E^3$, Ion identity library [maximum charge, 2; maximum molecules/cluster, 2; Adducts ($[M+H]^+$, $[M+Na]^+$, $[M+K]^+$, $[M+NH_4]^+$, $[M+2H]^{2+}$), Modifications ($[M-H_2O]$, $[M-2H_2O]$, $[M-CO_2]$, $[M+HFA]$, $[M+ACN]$)], Annotation refinement (Delete small networks without major ion, yes; Delete networks without monomer, yes), Add ion identities networks (*m/z* tolerance, 8 ppm; Minimum height, $1.0E^5$; Annotation refinement (Minimum size, 1; Delete small networks without major ion, yes; Delete small networks: Link threshold, 4; Delete networks without monomer, yes)) and Check all ion identities by MS/MS (*m/z* tolerance (MS^2)), 10 ppm; min-height (in MS^2), $1.0E^3$; Check for multimers, yes; Check neutral losses (MS^1 ->MS^2), yes) modules. The resulting aligned peak list was exported as a *.mgf* file for further analysis.

Spectral Organization through Molecular Networking.

A molecular network for HPE was constructed from the *.mgf* file exported from MZmine3, using the FBMN workflow on the GNPS platform (Wang et al., 2016; Nothias et al., 2020). The precursor ion mass tolerance was set to 0.02 Da with an MS^2 fragment ion tolerance of 0.02 Da. A network was created where edges were filtered to have a cosine score above 0.7 and more than six matched peaks. The spectra in the network were then searched against GNPS' spectral libraries. All matches between network and library spectra were required to have a score above 0.6, and at least three matched peaks. Job link: https://gnps.ucsd.edu/ProteoSAFe/status.jsp?task=c9e133b094404c0ab373c991b8924fb0

Taxonomically Informed Metabolite Annotation.

The *.mgf* file exported from MZmine3 was also annotated by spectral matching against an *in-silico* database to obtain putative annotations (Allard et al., 2016). The resulting annotations were subjected to taxonomically informed metabolite scoring (https://taxonomicallyinformedannotation.github.io/tima-r/, *v 2.8.2*) and re-ranking (Rutz et al., 2019) from the chemotaxonomic information available on LOTUS (Rutz et al., 2022). The *in-silico* database used for this process includes the combined records of the Dictionary of Natural Products (DNP, *v*30.2) and the LOTUS Initiative outputs.

SIRIUS Metabolite Annotation.

The SIRIUS *.mgf* file exported from MZmine3 (using the SIRIUS export module) that contains MS^1 and MS^2 information was processed with SIRIUS (v5.6.3) (Dührkop et al., 2019). The parameters were set as follows: Possible ionizations: $[M+H]^+$, $[M+NH_4]^+$, $[M-H_2O+H]^+$, $[M+K]^+$, $[M+Na]^+$, $[M-4H_2O+H]^+$; Instrument profile: Orbitrap; Mass accuracy: 5 ppm for MS^1 and 7 ppm for MS^2, the Database for molecular formulas and structures: BIO, Maximum *m/z* to compute: 1000. ZODIAC was used to improve molecular formula prediction using a threshold filter of 0.99 (Ludwig et al., 2020). Metabolite structure prediction was made with CSI: FingerID (Dührkop et al., 2015) and the significance was computed with COSMIC (Hoffmann et al., 2022). The chemical class prediction was made with CANOPUS (Dührkop et al., 2021) using the NPClassifier chemical taxonomy (Kim et al., 2021).

Wnt activity assessing assay.

Cell lines and culture conditions.

The BT-20, HCC1395 and HEK293 cell lines were cultured and utilized in experimental conditions in Dulbecco's Modified Medium (Thermo Fisher Scientific) supplemented with 10% Fetal Calf Serum and 1% penicillin-streptomycin at 37°C and 5% CO_2.

Luciferase-based assay of the Wnt-dependent transcriptional activity.

Purified Wnt3a was obtained from mouse L-cells stably transfected with Wnt3a, as previously described (Willert et al., 2003), with our own modifications (Xu et al., 2020). The three cell lines, stably transfected with the M50 Super 8×TopFlash plasmid, were seeded at a density of 6000 cells/well in white tissue-culture-treated 384-well plates in 20 μL/well maintenance medium. The cells were also transfected with the pCMV-RL plasmid to allow for constitutive expression of Renilla luciferase, using XtremeGENE 9 reagent according to the manufacturer's protocol. After 24 hours post-transfection, the medium was replaced with 2-fold indicated concentrations of compounds in 10 μL/well maintenance medium. Following a 1-hour preincubation, Wnt3a was added to a final concentration of 500 ng/mL in an additional 10 μL/well volume. After a further 24 hours of incubation, the medium was removed and measurements were taken using a Tecan Infinite M200 PRO plate reader equipped with a two-channel dispensing unit by injecting sequentially 15 μL of each of the buffer solutions for activity measurements of firefly and Renilla luciferase, as described previously (Boudou et al., 2022). The resulting dose-response data for this and the MTT assay were fitted using GraphPad Prism 9 software (v9.4.0, Boston, USA) to obtain IC_{50} values. Since the assay is designed to not use positive control compounds, an extract or compound is considered '*toxic*' if the IC50 value against Renilla luciferase is less than 1.7-fold of estimated TopFlash one, indicating that the decrease observed in TopFlash response is affected by a strong toxic effect.

Conclusions

The findings of this study demonstrate the potential of combining *Inventa*'s structural novelty scores with bioactivity results for guiding the discovery of structurally novel bioactive NPs in collections of NEs. Through the evaluation of Wnt-regulation activity results and *Inventa*'s scores, a collection of 1,600 NEs was narrowed down to four active NEs with a high potential of containing structural novel NPs. Based on additional criteria (*Similarity Score*, number of compounds reported at

the species and genus level) only one extract was selected. Although *Invent* a's novelty scores do not correlate directly with observed bioactivity, they play a crucial role in prioritizing NEs and reducing selection prior to in-depth phytochemical study. This approach reduces the risk of prioritizing known NPs and underlines the importance of employing the most comprehensive bioinformatics approaches rather than relying solely on bioactivity results as sample selection criteria. The subsequent phytochemical investigation of *Hymenocardia punctata* leaves led to the isolation of ten novel bicyclo[3.3.1]non-3-ene-2,9-diones and three known prenylated flavones. Some of the newly isolated compounds exhibited appreciable IC_{50} values and showed no apparent cytotoxicity in three different cell lines, indicating their potential as Wnt inhibitory compounds. This work illustrates the utility of *Inventa* in assisting the efficient selection of active NEs from large sample collections for the identification of novel and bioactive NPs.

Associated Content

Data and Code Availability

The *.mzML* and raw UHPLC-HMRMS[2] data for all the *H. punctata de novo* extract, can be accessed through MassIVE with the accession number MSV000092572. To access the molecular network follow the hyperlink: https://gnps.ucsd.edu/ProteoSAFe/status.jsp?task=c9e133b094404c0ab373c991b8924fb0 (PI). The ISDB and Sirius annotations (CSI:FingerID and CANOPUS) accessible here. Cytoscape files for the molecular network in positive ionization mode are available here.

The *.mzXML* and raw UHPLC-HMRMS[2] data of the original PFL 1600 NEs collection profiling can be visualized and downloaded here.

The standard workflow used for processing and generating the Feature-Based Molecular Networking can be found in the GNPS documentation. The workflow for ISDB annotation and taxonomical re-weighting can be found here. The script for cleaning and consolidating the annotations from GNPS can be found here.

The raw data files for the NMR and ECD (calculated and experimental) analysis are available at the following link: https://doi.org/10.26037/yareta:tnynbxbghrayrjqhnrzax4ijgi

Supporting Information

The Supplementary Material for this article can be found online at:

Table SI shows a resume of selected annotations for HPE extract in PI mode.

Table SII shows the Wnt-regulation bioactivity results for the pooled fraction derived from the micro fractionation of the HPE extract.

Figure S1 shows the Molecular Networking and dereplication results for *H. punctata* original extract.

Figure S2-S3 show the Molecular Networking and dereplication results for *H. punctata de novo* extracts.

Figure S4 describes the micro fractionation strategy.

Figure S5 shows the Tautomeric equilibrium present in compounds **2**, **8**, **10** and **11**.

Figure S6 shows the comparisons between the experimental and calculate Electronic Circular Dichroism (ECD) spectra for compounds **1-13** in methanol.

Figures S7 shows the Wnt-regulation bioactivity curves results for the active compounds **1**, **2**, **3**, **4** and **7**.

Figures S8– S84 show the 1D and 2D NMR analysis for the isolated compounds **1-13**.

Author Information

Conflict of interest disclosure

The authors declare no conflict of interest.

Author contributions

Conceptualization: L-M.Q-G, J-L.W. Plant material preparation and logistics: B.D, A.G. Preparation, sample acquisition, and data curation: L-M.Q-G, N.C. Isolation and structural elucidation: L-M.Q-G, N.C, L.M. Biological activity assessment: A.K, V.K. Software, and visualization: L-M.Q-G. Supervision: J-L.W. Funding acquisition: J-L.W. Writing—original draft: L-M.Q-G, L.M. Review and editing: L-M.Q-G, L.M, N.C, EFQ, A.G, A.K, V.K, J-L.W. All the authors have read and validated the final manuscript.

References

Allard, P.-M., Gaudry, A., Quirós-Guerrero, L.-M., Rutz, A., Dounoue-Kubo, M., Walker, T. W. N., et al. (2023). Open and reusable annotated mass spectrometry dataset of a chemodiverse collection of 1,600 plant extracts. *Gigascience* 12. doi: 10.1093/gigascience/giac124.

Allard, P.-M., Péresse, T., Bisson, J., Gindro, K., Marcourt, L., Pham, V. C., et al. (2016). Integration of Molecular Networking and In-Silico MS/MS Fragmentation for Natural Products Dereplication. *Anal. Chem.* 88, 3317–3323. doi: 10.1021/acs.analchem.5b04804.

Amado, N. G., Fonseca, B. F., Cerqueira, D. M., Neto, V. M., and Abreu, J. G. (2011). Flavonoids: potential Wnt/beta-catenin signaling modulators in cancer. *Life Sci.* 89, 545–554. doi: 10.1016/j.lfs.2011.05.003.

Amado, N. G., Predes, D., Moreno, M. M., Carvalho, I. O., Mendes, F. A., and Abreu, J. G. (2014). Flavonoids and Wnt/β-catenin signaling: potential role in colorectal cancer therapies. *Int. J. Mol. Sci.* 15, 12094–12106. doi: 10.3390/ijms150712094.

Atanasov, A. G., Zotchev, S. B., Dirsch, V. M., International Natural Product Sciences Taskforce, and Supuran, C. T. (2021). Natural products in drug discovery: advances and opportunities. *Nat. Rev. Drug Discov.* 20, 200–216. doi: 10.1038/s41573-020-00114-z.

Blagodatski, A., Klimenko, A., Jia, L., and Katanaev, V. L. (2020). Small molecule Wnt Pathway modulators from natural sources: History, state of the art and perspectives. *Cells* 9. doi: 10.3390/cells9030589.

Boudou, C., Mattio, L., Koval, A., Soulard, V., and Katanaev, V. L. (2022). Wnt-pathway inhibitors with selective activity against triple-negative breast cancer: From thienopyrimidine to quinazoline inhibitors. *Front. Pharmacol.* 13, 1045102. doi: 10.3389/fphar.2022.1045102.

Cabral, R. S., Allard, P.-M., Marcourt, L., Young, M. C. M., Queiroz, E. F., and Wolfender, J.-L. (2016). Targeted Isolation of Indolopyridoquinazoline Alkaloids from *Conchocarpus fontanesianus* Based on Molecular Networks. *J. Nat. Prod.* 79, 2270–2278. doi: 10.1021/acs.jnatprod.6b00379.

Caesar, L. K., Montaser, R., Keller, N. P., and Kelleher, N. L. (2021). Metabolomics and genomics in natural products research: complementary tools for targeting new chemical entities. *Nat. Prod. Rep.* 38, 2041–2065. doi: 10.1039/d1np00036e.

Clark, A. M. (1996). Natural products as a resource for new drugs. *Pharm. Res.* 13, 1133–1144. doi: 10.1023/a:1016091631721.

Dat, N. T., Binh, P. T. X., Quynh, L. T. P., Van Minh, C., Huong, H. T., and Lee, J. J. (2010). Cytotoxic prenylated flavonoids from *Morus alba*. *Fitoterapia* 81, 1224–1227. doi: 10.1016/j.fitote.2010.08.006.

David, B., Wolfender, J.-L., and Dias, D. A. (2015). The pharmaceutical industry and natural products: historical status and new trends. *Phytochem. Rev.* 14, 299–315. doi: 10.1007/s11101-014-9367-z.

Dias, D. A., Urban, S., and Roessner, U. (2012). A historical overview of natural products in drug discovery. *Metabolites* 2, 303–336. doi: 10.3390/metabo2020303.

Dührkop, K., Fleischauer, M., Ludwig, M., Aksenov, A. A., Melnik, A. V., Meusel, M., et al. (2019). SIRIUS 4: a rapid tool for turning tandem mass spectra into metabolite structure information. *Nat. Methods* 16, 299–302. doi: 10.1038/s41592-019-0344-8.

Dührkop, K., Nothias, L.-F., Fleischauer, M., Reher, R., Ludwig, M., Hoffmann, M. A., et al. (2021). Systematic classification of unknown metabolites using high-resolution fragmentation mass spectra. *Nat.*

Biotechnol. 39, 462–471. doi: 10.1038/s41587-020-0740-8.

Dührkop, K., Shen, H., Meusel, M., Rousu, J., and Böcker, S. (2015). Searching molecular structure databases with tandem mass spectra using CSI:FingerID. *Proc. Natl. Acad. Sci. U. S. A.* 112, 12580–12585. doi: 10.1073/pnas.1509788112.

Feher, M., and Schmidt, J. M. (2003). Property distributions: differences between drugs, natural products, and molecules from combinatorial chemistry. *J. Chem. Inf. Comput. Sci.* 43, 218–227. doi: 10.1021/ci0200467.

Fuentes, R. G., Arai, M. A., and Ishibashi, M. (2015). Natural compounds with Wnt signal modulating activity. *Nat. Prod. Rep.* 32, 1622–1628. doi: 10.1039/c5np00074b.

Fukai, T., Qing-Hua, W., and Nomura, T. (1991). Six prenylated phenols from *Glycyrrhiza uralensis.* *Phytochemistry* 30, 1245–1250. doi: 10.1016/S0031-9422(00)95210-5.

Fu, K.-L., Shen, Y.-H., Lu, L., Li, B., He, Y.-R., Li, B., et al. (2013). Two unusual rearranged flavan derivatives from *Narcissus tazetta* var. chinensis. *Helv. Chim. Acta* 96, 338–344. doi: 10.1002/hlca.201200248.

Gamache, P. H. (2017). *Charged Aerosol Detection for Liquid Chromatography and Related Separation Techniques*. John Wiley & Sons.

Gaudry, A., Huber, F., Nothias, L.-F., Cretton, S., Kaiser, M., Wolfender, J.-L., et al. (2022). MEMO: Mass Spectrometry-Based Sample Vectorization to explore chemodiverse datasets. *Front Bioinform* 2, 842964. doi: 10.3389/fbinf.2022.842964.

Gaudry, A., Pagni, M., Mehl, F., Moretti, S., Quiros-Guerrero, L.-M., Rutz, A., et al. (2023). A Sample-Centric and Knowledge-Driven Computational Framework for Natural Products Drug Discovery. *ChemRxiv*. doi: 10.26434/chemrxiv-2023-sljbt.

Guillarme, D., Nguyen, D. T. T., Rudaz, S., and Veuthey, J.-L. (2008). Method transfer for fast liquid chromatography in pharmaceutical analysis: application to short columns packed with small particle. Part II: gradient experiments. *Eur. J. Pharm. Biopharm.* 68, 430–440. doi: 10.1016/j.ejpb.2007.06.018.

Gu, J., Cui, C.-F., Yang, L., Wang, L., and Jiang, X.-H. (2019). Emodin Inhibits Colon Cancer Cell Invasion and Migration by Suppressing Epithelial-Mesenchymal Transition via the Wnt/β-Catenin Pathway. *Oncol. Res.* 27, 193–202. doi: 10.3727/096504018X15150662230295.

Hamburger, M. (2019). HPLC-based activity profiling for pharmacologically and toxicologically relevant natural products - principles and recent examples. *Pharm. Biol.* 57, 328–334. doi: 10.1080/13880209.2019.1606261.

Hanwell, M. D., Curtis, D. E., Lonie, D. C., Vandermeersch, T., Zurek, E., and Hutchison, G. R. (2012). Avogadro: an advanced semantic chemical editor, visualization, and analysis platform. *J. Cheminform.* 4, 17. doi: 10.1186/1758-2946-4-17.

Hoffmann, M. A., Nothias, L.-F., Ludwig, M., Fleischauer, M., Gentry, E. C., Witting, M., et al. (2022). High-confidence structural annotation of metabolites absent from spectral libraries. *Nat. Biotechnol.* 40, 411–421. doi: 10.1038/s41587-021-01045-9.

Hostettmann, K., and Terreaux, C. (2000). Search for new lead compounds from higher plants. *Chimia* 54, 652. doi: 10.2533/chimia.2000.652.

Houschyar, K. S., Tapking, C., Borrelli, M. R., Popp, D., Duscher, D., Maan, Z. N., et al. (2018). Wnt

Pathway in bone repair and regeneration - What do we know so far. *Front Cell Dev Biol* 6, 170. doi: 10.3389/fcell.2018.00170.

Huber, F., Ridder, L., Verhoeven, S., Spaaks, J. H., Diblen, F., Rogers, S., et al. (2021). Spec2Vec: Improved mass spectral similarity scoring through learning of structural relationships. *PLoS Comput. Biol.* 17, e1008724. doi: 10.1371/journal.pcbi.1008724.

Huber, F., Verhoeven, S., Meijer, C., Spreeuw, H., Castilla, E., Geng, C., et al. (2020). Matchms - processing and similarity evaluation of mass spectrometry data. *J. Open Source Softw.* 5, 2411. doi: 10.21105/joss.02411.

Hubert, J., Nuzillard, J.-M., and Renault, J.-H. (2017). Dereplication strategies in natural product research: How many tools and methodologies behind the same concept? *Phytochem. Rev.* 16, 55–95. doi: 10.1007/s11101-015-9448-7.

Hulstaert, N., Shofstahl, J., Sachsenberg, T., Walzer, M., Barsnes, H., Martens, L., et al. (2020). ThermoRawFileParser: Modular, Scalable, and Cross-Platform RAW File Conversion. *J. Proteome Res.* 19, 537–542. doi: 10.1021/acs.jproteome.9b00328.

Ibrahim, H., Sani, F. S., Danladi, B. H., and Ahmadu, A. A. (2007). Phytochemical and antisickling studies of the leaves of *Hymenocardia acida* Tul (Euphorbiaceae). *Pak. J. Biol. Sci.* 10, 788–791. doi: 10.3923/pjbs.2007.788.791.

Inestrosa, N. C., Montecinos-Oliva, C., and Fuenzalida, M. (2012). Wnt signaling: role in Alzheimer disease and schizophrenia. *J. Neuroimmune Pharmacol.* 7, 788–807. doi: 10.1007/s11481-012-9417-5.

Jiang, H., Zhang, Z., Yu, Y., Chu, H. Y., Yu, S., Yao, S., et al. (2022). Drug Discovery of DKK1 Inhibitors. *Front. Pharmacol.* 13, 847387. doi: 10.3389/fphar.2022.847387.

Khiari, R., Baaka, N., Ammar, M., and Saad, M. K. (2017). Properties of tannin-glyoxal resins prepared from lyophilized and condensed tannin. *J. Text. Eng. Fash. Technol.* 3, 62–65. doi: 10.15406/jteft.2017.03.00110.

Kim, H. W., Wang, M., Leber, C. A., Nothias, L.-F., Reher, R., Kang, K. B., et al. (2021). NPClassifier: A Deep Neural Network-Based Structural Classification Tool for Natural Products. *J. Nat. Prod.* 84, 2795–2807. doi: 10.1021/acs.jnatprod.1c00399.

Koval, A. V., Vlasov, P., Shichkova, P., Khunderyakova, S., Markov, Y., Panchenko, J., et al. (2014). Anti-leprosy drug clofazimine inhibits growth of triple-negative breast cancer cells via inhibition of canonical Wnt signaling. *Biochem. Pharmacol.* 87, 571–578. doi: 10.1016/j.bcp.2013.12.007.

Landesman-Bollag, E., Song, D. H., Romieu-Mourez, R., Sussman, D. J., Cardiff, R. D., Sonenshein, G. E., et al. (2001). Protein kinase CK2: signaling and tumorigenesis in the mammary gland. *Mol. Cell. Biochem.* 227, 153–165. Available at: https://www.ncbi.nlm.nih.gov/pubmed/11827167.

Ligor, M., Studzińska, S., Horna, A., and Buszewski, B. (2013). Corona-Charged Aerosol Detection: An Analytical Approach. *Crit. Rev. Anal. Chem.* 43, 64–78. doi: 10.1080/10408347.2012.746134.

Lim, H. Y., Ong, P. S., Wang, L., Goel, A., Ding, L., Li-Ann Wong, A., et al. (2021). Celastrol in cancer therapy: Recent developments, challenges and prospects. *Cancer Lett.* 521, 252–267. doi: 10.1016/j.canlet.2021.08.030.

Lin, M., Cai, P.-J., Zeng, Z., Lin, N., Shen, Y., Tang, B., et al. (2018). Conformational bias by a removable silyl group: Construction of bicyclo[n.3.1]alkenes by ring closing metathesis. *Chemistry* 24, 2334–2338. doi: 10.1002/chem.201705275.

Lin, Y., Kuang, Y., Li, K., Wang, S., Ji, S., Chen, K., et al. (2017). Nrf2 activators from *Glycyrrhiza inflata* and their hepatoprotective activities against CCl4-induced liver injury in mice. *Bioorg. Med. Chem.* 25, 5522–5530. doi: 10.1016/j.bmc.2017.08.018.

Liu, J., Xiao, Q., Xiao, J., Niu, C., Li, Y., Zhang, X., et al. (2022). Wnt/β-catenin signalling: function, biological mechanisms, and therapeutic opportunities. *Signal Transduct Target Ther* 7, 3. doi: 10.1038/s41392-021-00762-6.

Lojk, J., and Marc, J. (2021). Roles of non-Canonical Wnt signalling pathways in bone biology. *Int. J. Mol. Sci.* 22. doi: 10.3390/ijms221910840.

Mali, R. G., and Wadekar, R. R. (2008). In Vitro Anthelmintic Activity of *Baliospermum montanum* Muell. Arg roots. *Indian J. Pharm. Sci.* 70, 131–133. doi: 10.4103/0250-474X.40352.

Mándi, A., and Kurtán, T. (2019). Applications of OR/ECD/VCD to the structure elucidation of natural products. *Nat. Prod. Rep.* 36, 889–918. doi: 10.1039/c9np00002j.

Nagoya Protocol on access to genetic resources and the fair and equitable sharing of benefits arising from their utilization to the convention of biological diversity (2011). *Nagoya Protocol on Access to Genetic Resources and the Fair and Equitable Sharing of Benefits Arising from Their Utilization to the Convention of Biological Diversity*. Available at: https://treaties.un.org/pages/ViewDetails.aspx?src=IND&mtdsg_no=XXVII-8-b&chapter=27&clang=_en [Accessed October 29, 2022].

Najmi, A., Javed, S. A., Al Bratty, M., and Alhazmi, H. A. (2022). Modern approaches in the discovery and development of plant-based natural products and their analogues as potential therapeutic agents. *Molecules* 27. doi: 10.3390/molecules27020349.

Nanna, U., Chularojmontri, L., Tingpej, P., Kaewamatawong, R., Homhual, S., Suwannaloet, W., et al. (2021). Effect of *Aporosa villosa* stem ethanolic extract on adipogenesis in 3T3-L1 adipocytes. *Pharmacogn. J.* 13, 1422–1427. doi: 10.5530/pj.2021.13.180.

Newman, D. J., and Cragg, G. M. (2020). Natural products as sources of new drugs over the nearly four decades from 01/1981 to 09/2019. *J. Nat. Prod.* 83, 770–803. doi: 10.1021/acs.jnatprod.9b01285.

Nothias, L.-F., Petras, D., Schmid, R., Dührkop, K., Rainer, J., Sarvepalli, A., et al. (2020). Feature-based molecular networking in the GNPS analysis environment. *Nat. Methods* 17, 905–908. doi: 10.1038/s41592-020-0933-6.

Nugroho, A. E., and Morita, H. (2014). Circular dichroism calculation for natural products. *J. Nat. Med.* 68, 1–10. doi: 10.1007/s11418-013-0768-x.

Nusse, R., and Clevers, H. (2017). Wnt/β-Catenin signaling, disease, and emerging therapeutic modalities. *Cell* 169, 985–999. doi: 10.1016/j.cell.2017.05.016.

Ogura, M., Koike, K., Cordell, G. A., and Farnsworth, N. R. (1978). Potential anticancer agents VIII. Constituents of *Baliospermum montanum* (Euphorbiaceae). *Planta Med.* 33, 128–143. doi: 10.1055/s-0028-1097367.

Olivon, F., Grelier, G., Roussi, F., Litaudon, M., and Touboul, D. (2017). MZmine 2 Data-Preprocessing To Enhance Molecular Networking Reliability. *Anal. Chem.* 89, 7836–7840. doi: 10.1021/acs.analchem.7b01563.

Pieters, L., and Vlietinck, A. J. (2005). Bioguided isolation of pharmacologically active plant components, still a valuable strategy for the finding of new lead compounds? *J. Ethnopharmacol.* 100, 57–60. doi:

10.1016/j.jep.2005.05.029.

Pooja, T., and Karunagaran, D. (2014). Emodin suppresses Wnt signaling in human colorectal cancer cells SW480 and SW620. *Eur. J. Pharmacol.* 742, 55–64. doi: 10.1016/j.ejphar.2014.08.028.

Qiu, Z.-C., Zhang, Y., Xiao, H.-H., Chui-Wa Poon, C., Li, X.-L., Cui, J.-F., et al. (2020). 8-prenylgenistein exerts osteogenic effects via ER α and Wnt-dependent signaling pathway. *Exp. Cell Res.* 395, 112186. doi: 10.1016/j.yexcr.2020.112186.

Queiroz, E. F., Alfattani, A., Afzan, A., Marcourt, L., Guillarme, D., and Wolfender, J.-L. (2019). Utility of dry load injection for an efficient natural products isolation at the semi-preparative chromatographic scale. *J. Chromatogr. A* 1598, 85–91. doi: 10.1016/j.chroma.2019.03.042.

Quiros-Guerrero, L.-M., Nothias, L.-F., Gaudry, A., Marcourt, L., Allard, P.-M., Rutz, A., et al. (2022). *Inventa*: A computational tool to discover structural novelty in natural extracts libraries. *Front Mol Biosci* 9, 1028334. doi: 10.3389/fmolb.2022.1028334.

Rajaonarivelo, M., Rakotonandrasana, O. L., Martin, M.-T., Dumontet, V., and Rasoanaivo, P. (2016). A new polycyclic polyprenylated acylphloroglucinol derivative from *Garcinia verrucosa*. *Nat. Prod. Commun.* 11, 1005–1007. Available at: https://www.ncbi.nlm.nih.gov/pubmed/30452183.

Rutz, A., Dounoue-Kubo, M., Ollivier, S., Bisson, J., Bagheri, M., Saesong, T., et al. (2019). Taxonomically informed scoring enhances confidence in natural products annotation. *Front. Plant Sci.* 10, 1329. doi: 10.3389/fpls.2019.01329.

Rutz, A., Sorokina, M., Galgonek, J., Mietchen, D., Willighagen, E., Gaudry, A., et al. (2022). The LOTUS initiative for open knowledge management in natural products research. *Elife* 11, 2021.02.28.433265. doi: 10.7554/eLife.70780.

Sarker, S. D., Latif, Z., and Gray, A. I. (2005). *Natural Products Isolation*. , ed. Satyajit D. Sarker Zahid Latif Alexander I. Gray 999 Riverview Drive, Suite 208, Totowa, New Jersey 07512: Springer Science & Business Media.

Sarker, S. D., and Nahar, L. (2012). An introduction to natural products isolation. *Methods Mol. Biol.* 864, 1–25. doi: 10.1007/978-1-61779-624-1_1.

Schmid, R., Heuckeroth, S., Korf, A., Smirnov, A., Myers, O., Dyrlund, T. S., et al. (2023). Integrative analysis of multimodal mass spectrometry data in MZmine 3. *Nat. Biotechnol.* 41, 447–449. doi: 10.1038/s41587-023-01690-2.

Schmid, R., Petras, D., Nothias, L.-F., Wang, M., Aron, A. T., Jagels, A., et al. (2021). Ion identity molecular networking for mass spectrometry-based metabolomics in the GNPS environment. *Nat. Commun.* 12, 3832. doi: 10.1038/s41467-021-23953-9.

Sears, K. D., Casebier, R. L., Hergert, H. L., Stout, G. H., and McCandlish, L. E. (1974). Structure of catechinic acid. Base rearrangement product of catechin. *J. Org. Chem.* 39, 3244–3247. doi: 10.1021/jo00936a015.

Seigler, D. S. (1994). Phytochemistry and Systematics of the Euphorbiaceae. *Ann. Mo. Bot. Gard.* 81, 380–401. doi: 10.2307/2992104.

Selegato, D. M., Zanatta, A. C., Pilon, A. C., Veloso, J. H., and Castro-Gamboa, I. (2023). Application of feature-based molecular networking and MassQL for the MS/MS fragmentation study of depsipeptides. *Front. Mol. Biosci.* 10. doi: 10.3389/fmolb.2023.1238475.

Shaw, H. V., Koval, A., and Katanaev, V. L. (2019a). A high-throughput assay pipeline for specific targeting of frizzled GPCRs in cancer. *Methods Cell Biol.* 149, 57–75. doi: 10.1016/bs.mcb.2018.08.006.

Shaw, H. V., Koval, A., and Katanaev, V. L. (2019b). Targeting the Wnt signalling pathway in cancer: prospects and perils. *Swiss Med. Wkly* 149, w20129. doi: 10.4414/smw.2019.20129.

Song, D. H., Sussman, D. J., and Seldin, D. C. (2000). Endogenous protein kinase CK2 participates in Wnt signaling in mammary epithelial cells. *J. Biol. Chem.* 275, 23790–23797. doi: 10.1074/jbc.M909107199.

Srikrishna, L. P., Vagdevi, H. M., Basavaraja, B. M., and Vaidya, V. P. (2008). Evaluation of antimicrobial and analgesic activities of Aporosa lindleyana (euphorbiaceae) bark extract. *International Journal of Green Pharmacy (IJGP)* 2. doi: 10.22377/ijgp.v2i3.22.

Stevens, J. F. (2020). "Xanthohumol and structurally related prenylflavonoids for cancer chemoprevention and control," in *Natural Products for Cancer Chemoprevention: Single Compounds and Combinations*, eds. J. M. Pezzuto and O. Vang (Cham: Springer International Publishing), 319–350. doi: 10.1007/978-3-030-39855-2_10.

Takashima, J., and Ohsaki, A. (2001). Acutifolins A-F, a new flavan-derived constituent and five new flavans from *Brosimum acutifolium*. *J. Nat. Prod.* 64, 1493–1496. doi: 10.1021/np010389j.

The Angiosperm Phylogeny Group (2009). An update of the Angiosperm Phylogeny Group classification for the orders and families of flowering plants: APG III. *Bot. J. Linn. Soc.* 161, 105–121. doi: 10.1111/j.1095-8339.2009.00996.x.

Traven, V. F., Negrebetsky, V. V., Vorobjeva, L. I., and Carberry, E. A. (1997). Keto–enol tautomerism, NMR spectra, and H–D exchange of 4-hydroxycoumarins. *Can. J. Chem.* 75, 377–383. doi: 10.1139/v97-043.

van Welzen, P. C. (2016). *Bischofia* and *Hymenocardia* (Phyllanthaceae) in Malesia. *Blumea - Biodiversity, Evolution and Biogeography of Plants* 61, 272–279. doi: 10.3767/000651916X694337.

Venkataraman, R., Gopalakrishnan, S., Thyagarajan, S. P., and Others (2010). Antiviral activities of *Aporosa lindleyana* Baill. *Ann. Biol. Res.* 1, 68–70.

Wang, M., Carver, J. J., Phelan, V. V., Sanchez, L. M., Garg, N., Peng, Y., et al. (2016). Sharing and community curation of mass spectrometry data with Global Natural Products Social Molecular Networking. *Nat. Biotechnol.* 34, 828–837. doi: 10.1038/nbt.3597.

Willert, K., Brown, J. D., Danenberg, E., Duncan, A. W., Weissman, I. L., Reya, T., et al. (2003). Wnt proteins are lipid-modified and can act as stem cell growth factors. *Nature* 423, 448–452. doi: 10.1038/nature01611.

Xu, J., Koval, A., and Katanaev, V. L. (2020). Beyond TNBC: Repositioning of Clofazimine against a broad range of Wnt-dependent cancers. *Front. Oncol.* 10, 602817. doi: 10.3389/fonc.2020.602817.

Yazaki, K., Sasaki, K., and Tsurumaru, Y. (2009). Prenylation of aromatic compounds, a key diversification of plant secondary metabolites. *Phytochemistry* 70, 1739–1745. doi: 10.1016/j.phytochem.2009.08.023.

Zhang, H., Tao, L., Fu, W.-W., Liang, S., Yang, Y.-F., Yuan, Q.-H., et al. (2014). Prenylated benzoylphloroglucinols and xanthones from the leaves of *Garcinia oblongifolia* with antienteroviral activity. *J. Nat. Prod.* 77, 1037–1046. doi: 10.1021/np500124e.

Zhang, Y., Zhou, L.-P., Li, X.-L., Zhao, Y.-J., Ho, M.-X., Qiu, Z.-C., et al. (2018). 8-Prenylgenistein, a prenylated genistein derivative, exerted tissue selective osteoprotective effects in ovariectomized mice.

Oncotarget 9, 24221–24236. doi: 10.18632/oncotarget.24823.

Zhou, K., Yang, S., and Li, S.-M. (2021). Naturally occurring prenylated chalcones from plants: structural diversity, distribution, activities and biosynthesis. *Nat. Prod. Rep.* 38, 2236–2260. doi: 10.1039/d0np00083c.

Table 1. ^{1}H NMR (600 MHz) and ^{13}C NMR (151 MHz) data of compounds 1, 2, 4, 6, and 8 in CD_3OD. NA: signal not detected due to the keto-enol tautomerism in the system C(5)-C(6)-C(7)

No.	Compound 1		Compound 2		Compound 4		Compound 6		Compound 8	
	δ_H (multi, J in Hz)	δ_C	δ_H (multi, J in Hz)	δ_C	δ_H (multi, J in Hz)	δ_C	δ_H (multi, J in Hz)	δ_C	δ_H (multi, J in Hz)	δ_C
2ax eq	3.12 (d, 5.4)	55.2	3.07 (d, 6.4)	53.8	-3.40 (d, 6.4)	49.4	3.03 (d, 6.2)	55.0	3.12 (d, 6.4)	53.6
3ax eq	2.28 (m) 1.64 (overlapped)	27.5	2.34 (tt, 14.3,5.8) 1.55 (overlapped)	28.1	2.36 (tt, 15.0, 14.1, 6.4, 5.0) 1.67 (overlapped)	27.8	2.26 (tt, 14.2, 5.6) 1.55 (brd, 10.8)	27.3	2.31 (tt, 13.8, 6.4) 1.56 (overlapped)	27.8
4ax eq	2.29 (m) 2.16 (overlapped)	33.1	2.17 (td, 13.8,4.9) 1.79 (dd, 13.8,5.2)	34.7	2.08 (td, 14.1,4.8) 1.78 (overlapped)	34.9	2.09 (td, 14.5, 4.6) 2.63 (dd, 14.5, 4.9)	36.2	2.17 (td, 13.8, 4.7) 1.79 (overlapped)	34.5
5	-	181.2	-	NO	-	200.7	-	176.5	-	NO
6	5.80 (s)	104.3	NO	NO	5.81 (s)	104.7	5.88 (s)	114.7	NO	NO
7	-	201.3	-	NO	-	182.1	-	200.7	-	NO
8	-	67.2	-	64.7	-	64.7	-	67.5	-	64.4
9	-	207.7	-	211.5	-	208.0	-	209.7	-	210.4
10	-	61.7	-	61.6	-	64.4	-	51.6	-	61.7
11	2.17 (dd, 14.3, 7.9) 2.05 (dd, 14.3, 6.0)	30.4	2.09 (m) 2.09 (m)	30.3	2.53 (m) 1.74 (overlapped)	28.7	2.15 (dd, 14.7,7.8) 2.07 (overlapped)	30.5	2.15 (overlapped) 2.08 (dd, 14.2,5.2)	30.1
12	4.76 (thept, 7.9, 6.0, 1.2)	121.1	4.87 (overlapped)	122.0	4.62 (dd, 11.1,5.4)	92.2	4.81 (thept, 7.8, 1.4)	121.2	4.87 (overlapped)	121.4

Position										
13	-	134.1	-	133.2	-	71.1	-	134.0		133.8
14	1.48 (d, 1.2)	18.0	1.47 (d, 1.5)	18.0	1.28 (s)	26.3	1.47 (d, 1.4)	18.0	1.46 (d, 1.5)	18.0
15	1.50 (d, 1.2)	26.1	1.55 (d, 1.5)	26.1	1.10 (s)	25.2	1.53 (d, 1.4)	26.1	1.55 (d, 1.5)	26.1
16	2.82 (t, 12.9, 10.9) 1.91 (dd, 12.9, 5.5)	30.8	2.57 (dd, 14.5, 6.9) 2.47 (dd, 14.5, 6.9)	31.1	2.53 (m) 2.43 (dd, 14.5, 6.9)	31.1	2.94 (dd, 14.9, 3.9) 1.74 (dd, 14.9, 5.3)	31.5	2.58 (dd, 14.5, 7.1) 2.49 (dd, 14.5, 7.1)	30.9
17	4.72 (dd, 10.9, 5.5)	92.8	5.19 (thept, 6.9, 1.5)	121.9	5.07 (brt, 7.3)	121.1	3.79 (t, 5.3, 3.9)	69.9	5.19 (thept, 7.1, 1.5)	121.4
18	-	71.1	-	133.9	-	134.5	-	84.8	-	134.4
19	1.34 (s)	26.5	1.70 (d, 1.5)	18.2	1.68 (s)	18.2	1.44 (s)	24.0	1.68 (d, 1.4)	18.2
20	1.21 (s)	25.4	1.68 (d, 1.5)	26.1	1.63 (s)	26.1	1.26 (s)	26.9	1.70 (d, 1.4)	26.2
1'	-	137.9	-	133.4	-	138.1	-	138.1	-	138.2
2'	6.38 (d, 2.3)	121.6	6.28 (d, 2.2)	121.4	6.53 (d, 2.2)	115.9	6.31 (d, 2.3)	121.4	6.34 (d, 2.3)	121.6
3'	-	136.3	-	129.4	-	136.7	-	136.2	-	136.2
4'	-	146.0	-	143.0	-	146.1	-	145.9	-	145.9
5'	-	151.0	-	145.8	-	151.4	-	151.0	-	150.9
6'	6.47 (d, 2.3)	115.8	6.38 (d, 2.2)	114.8	6.43 (d, 2.2)	121.3	6.42 (d, 2.3)	116.1	6.44 (d, 2.3)	116.2
1''	3.28 (m) 3.28 (m)	29.1	3.25 (m) 3.25 (m)	29.2	3.28 (d, 7.4)	29.2	3.28 (d, 7.5)	29.0	3.27 (m) 3.27 (m)	29.3
2''	5.24 (thept, 6.7, 1.3)	123.9	5.30 (thept, 7.4, 1.4)	123.9	5.23 (brt, 7.4)	123.8	5.25 (thept, 7.5, 1.3)	123.8	5.25 (thept, 7.5, 1.4)	124.0

Position										
3''	-	133.6	-	133.2	-	133.6	-	133.8	-	133.4
4''	1.73 (d, 1.3)	17.9	1.72 (d, 1.4)	17.9	1.73 (s)	18.0	1.74 (d, 1.3)	17.9	1.74 (d, 1.4)	18.0
5''	1.77 (d, 1.3)	26.0	1.76 (d, 1.4)	26.0	1.76 (s)	26.0	1.79 (d, 1.3)	26.1	1.76 (d, 1.4)	26.0
4'OMe	3.75 (s)	60.8			3.74 (s)	60.8	3.75 (s)	60.8	3.74 (s)	60.8

Table 2. ^{1}H NMR (600 MHz) and ^{13}C NMR (151 MHz) data of compounds 9–13 in CD$_3$OD. NA: signal not detected due to the keto-enol tautomerism in the system C(5)-C(6)-C(7).

No.	Compound 9 δ_H (multi, J in Hz)	δ_C	Compound 10 δ_H (multi, J in Hz)	δ_C	Compound 11 δ_H (multi, J in Hz)	δ_C	Compound 12 δ_H (multi, J in Hz)	δ_C	Compound 13 δ_H (multi, J in Hz)	δ_C
2ax eq	3.63 (d, 6.2)	51.9	2.64 (dd, 13.2,4.0) -	56.2	2.68 (dd, 13.1, 4.0) -	55.7	- 3.04 (d, 6.2)	54.7	- 3.14 (d, 3.8)	55.3
3ax eq	2.36 (tt, 14.2, 6.2, 4.7) 1.53 (dt, 14.2, 4.7, 2.1)	27.5	2.21 (m) 1.71 (overlapped)	28.1	2.25 (td, 13.1, 4.8) 1.71 (overlapped)	28.2	2.23 (m) 1.63 (m)	27.6	2.32 (overlapped) 1.66 (m)	27.6
4ax eq	2.11 (td, 14.2,4.7) 1.64 (ddd, 14.2, 4.7, 2.1)	33.5	1.64 (overlapped) 1.97 (ddd, 13.1, 4.9, 1.8)	39.2	1.63 (overlapped) 1.98 (ddd, 12.9, 4.8, 1.8)	39.0	1.96 (td, 13.3,4.5) 2.28 (dd, 13.3, 4.5)	33.2	2.30 (overlapped) 2.23 (brd, 9.4)	32.6
5	-	200.2	-	NO	-	NO	-	176.8	-	NO
6	5.89 (s)	115.7	NO	NO	NO	NO	5.82 (s)	113.8	5.80 (s)	104.2
7	-	177.4	-	NO	-	NO	-	200.4	-	201.3
8	-	55.3					-	67.8	-	67.3
9	-	209.7	-	211.0	-	211.1	-	210.3	-	207.8
10	-	65.0					-	51.0	-	61.7
11	2.61 (dd, 14.7,3.9) 1.59 (dd, 14.7,7.8)	28.7	2.30 (dd, 15.0,6.7) 2.21 (m)	29.8	2.32 (dd, 14.9, 7.2) 2.18 (dd, 14.9, 7.2)	29.7	2.16 (dd, 14.7, 7.8) 2.06 (dd, 14.7, 6.1)	30.3	2.17 (dd, 14.5,7.7) 2.07 (dd, 14.5,6.0)	30.5
12	3.49 (dd, 7.8,3.9)	70.5	4.87 (overlapped)	121.9	4.89 (overlapped)	122.0	4.83 (thept, 7.6, 1.3)	121.3	4.78 (ddhept, 7.7, 6.0, 1.4)	121.0
13	-	85.3	-	133.3	-	133.1				134.2

Position	δH	δC	δH	δC	δH	δC	δH	δC	δH	δC
14	1.40 (s)	22.9	1.51 (d, 1.5)	18.2	1.51 (d, 1.6)	18.2	1.47 (d, 1.3)	17.9	1.49 (d, 1.4)	17.9
15	1.26 (s)	27.1	1.59 (d, 1.5)	26.1	1.60 (d, 1.6)	26.1	1.54 (d, 1.3)	26.0	1.53 (d, 1.4)	26.0
16	2.54 (dd, 14.5,7.7) 2.44 (dd, 14.5,6.8)	30.8	2.48 (m) 2.48 (m)	30.9	2.50 (dd, 14.3, 7.0) 2.46 (dd, 14.3, 7.0)	31.0	2.56 (td, 14.4, 4.2) 1.71 (dt, 14.4, 4.2)	24.2	2.63 (dd, 13.0, 11.2) 2.12 (dd, 13.0, 5.4)	35.4
17	5.17 (thept, 7.7, 6.8, 1.3)	121.2	4.97 (thept, 6.9, 1.5)	121.4	4.98 (thept, 7.0, 1.6)	121.6	2.04 (td, 14.3, 4.1) 1.86 (dt, 14.3, 4.1)	31.2	5.32 (dd, 11.2 5.4)	89.2
18	-	134.7	-	134.0	-	134.1	-	82.3	-	143.1
19	1.69 (d, 1.3)	18.2	1.69 (d, 1.5)	18.2	1.69 (d, 1.3)	18.2	1.46 (s)	30.1	1.78 (t, 1.2)	17.3
20	1.68 (d, 1.3)	26.2	1.63 (d, 1.5)	26.1	1.63 (d, 1.3)	26.1	1.29 (s)	26.2	5.17 (q, 1.2) 5.05 (q, 1.2)	114.4
1'	-	138.2	-	131.3	-	136.6	-	138.1	-	137.9
2'	6.31 (d, 2.3)	121.5	6.32 (d, 2.2)	122.6	6.38 (d, 2.2)	122.9	6.31 (d, 2.3)	121.4	6.38 (d, 2.3)	121.6
3'	-	136.4	-	128.7	-	135.4	-	136.3	-	136.4
4'	-	146.0	-	143.4	-	146.2	-	145.9	-	146.0
5'	-	151.3	-	145.3	-	150.4	-	151.0	-	151.1
6'	6.46 (d, 2.3)	116.9	6.40 (d, 2.2)	114.4	6.47 (d, 2.2)	116.0	6.41 (d, 2.3)	115.9	6.47 (d, 2.3)	115.8
1''	3.27 (m) 3.27 (m)	29.4	3.28 (dd, 15.6,7.4) 3.23 (dd, 15.6,7.4)	29.2	3.27 (m) 3.27 (m)	29.4	3.28 (m) 3.28 (m)	29.0	3.27 (m) 3.27 (m)	29.1
2''	5.24 (thept, 8.1, 1.3)	124.0	5.29 (thept, 7.4, 1.4)	124.2	5.24 (thept, 7.2, 1.3)	124.5	5.24 (thept, 7.5, 1.3)	123.8	5.25 (thept, 7.5, 1.3)	123.9

3"	-	133.6	-	132.7	-	132.9	-	134.0	-	133.5
4"	1.74 (d, 1.3)	18.0	1.71 (d, 1.4)	17.9	1.73 (d, 1.3)	18.0	1.73 (d, 1.3)	18.0	1.73 (d, 1.3)	18.0
5"	1.77 (d, 1.3)	26.0	1.73 (d, 1.4)	26.0	1.73 (d, 1.3)	25.9	1.78 (d, 1.3)	26.1	1.77 (d, 1.3)	26.1
4'OMe	3.73 (s)	60.7			3.73 (s)	60.7	3.74 (s)	60.8	3.75 (s)	60.8

Table 3. Wnt-inhibition assay results IC$_{50}$ (μM) for the isolated compounds **1-4** and **7**.

Compound	HCC1395	BT-20	HEK293
1	15.0 ± 0.3	51 ± 25	35 ± 1
2	17 ± 1	28 ± 10	26 ± 4
3	13 ± 1	27 ± 8	40.0 ± 0.2
4	14.0 ± 0.1	26 ± 1	31 ± 1
7	17 ± 5	16 ± 11	12 ± 2